# Quantification of Atg18 localization and Asymmetric Localization of Atg18 on the Daughter Vacuole of Budding Yeast

by

Mukadder Koyuncu

A Dissertation Submitted to the
Graduate School of Sciences and Engineering

in Partial Fulfillment of the Requirements for

the Degree of

Master of Science

in

Molecular Biology and Genetics


September 20, 2023

# Quantification of Atg18 localization and Asymmetric Localization of Atg18 on the Daughter Vacuole of Budding Yeast

Koç University

Graduate School of Sciences and Engineering

This is to certify that I have examined this copy of a master's thesis by

**Mukadder Koyuncu**

and have found that it is complete and satisfactory in all respects,

and that any and all revisions required by the final

examining committee have been made.

Committee Members:

---

Assist. Prof. Ayşe Koca Çaydaşı (Advisor – Koç University)

---

Prof. Halil Kavaklı (Koç University)

---

Prof. Zeynep Petek Çakar (Istanbul Technical University)

---

Date: 22/09/2023

*[To every character became a part of my story]*

# ABSTRACT

**Quantification of Atg18 localization and Asymmetric Localization of Atg18 on the Daughter Vacuole of Budding Yeast**

**Mukadder Koyuncu**

**Master of Science in Molecular Biology and Genetics**

**September 22, 2023**

Phospholipids play a key role in intracellular signaling. Membrane-bound phosphatidylinositols (PIs) are examples of those signaling lipids. They are phosphorylated from three different places, and these phosphorylations attract different proteins. In this thesis, phosphatidylinositol 3, 5 biphosphate $PI(3,5)P_2$ was investigated. The autophagy protein Atg18 localize on vacuole membranes in a way that correlates with $PI(3,5)P_2$ levels on the vacuoles. Therefore, if Atg18 can be utilized as a $PI(3,5)P_2$ marker is inquired. To quantify Atg18 localization on the vacuoles, the EzColocalization plugin was used in ImageJ-FIJI. This plugin provided us with a Pearson Correlation Coefficient, which indicates the amplitude of Atg18 localization on the vacuole. The deletion of $PI(3,5)P_2$ regulatory complex proteins, *VAC7*, *VAC14*, and *FAB1,* was investigated along with Atg18 mutants that either can only bind $PI(3,5)P_2$, or cannot bind any PI at all. The quantified results showed that Atg18 localization on vacuoles, indeed, increases with elevated $PI(3,5)P_2$ levels. Moreover, it was observed that Atg18 localizes only to the daughter vacuole after the vacuole segregates to the daughter cell. Using the EzColocalization plugin, I was able to show this phenomenon in numbers. Through several analyses, I found that daughter-specific Atg18 localization to the daughter vacuole mostly starts right after vacuole segregation ends, within 5 minutes around metaphase-anaphase transition, and ends 5 minutes after the spindle breakdown, persisting on daughter vacuole for 30 minutes on average. 49% of the mid-log phase population showed sole Atg18 daughter-specific localization from the end of vacuole segregation until cytokinesis, while more than 95% of the population showed daughter-specific Atg18 localization at some point. Whether other $PI(3,5)P_2$ regulators show asymmetry was also investigated. Timelapse of Vac14 showed no asymmetry. Population analysis of cells by measuring fluorescence intensity of still images also showed that Vac7, Vac14,

and Fab1 do not localize asymmetrically. On the other hand, two more proteins, Sch9 and Ivy1, were also analyzed since they are relevant to PI(3,5)$P_2$ signaling. Sch9 was slightly enriched on the mother vacuole, whereas Ivy1 was strongly enriched on the daughter vacuole. Atg18-Sloop mutant that only binds PI(3,5)$P_2$, was enriched on the daughter vacuole as well. Altogether, the findings of this thesis suggest that Atg18 vacuole localization correlates with the PI(3,5)$P_2$ production and it is likely that it may reflect PI(3,5)$P_2$ levels. This thesis also further presents evidence that the daughter and the mother vacuole exhibits compartment specific behavior in terms of some PI(3,5)P effectors (Atg18, Sch9) and regulators (Atg18 and Ivy1).

# ÖZETÇE

## Atg18 Proteinin Kofula Konumlanmasının Sayıya Dökümü ve Atg18 Proteinin Ekmek Mayasının Yavru Kofuluna Özgül Asimetrik Olarak Bağlanması

**Mukadder Koyuncu**

**Moleküler Biyoloji ve Genetik, Yüksek Lisans**

**22 Eylül 2023**

Fosfolipidler hücre içi iletişimde anahtar bir role sahiptir. Zara bağlı fosfatidilinositoler (PI) bu iletişim moleküllerinin bir örneğidir. Bu lipidler altı karbonlu inositol halkasının üç, dört ve beşinci karbonlarından fosforlanmasıyla farklı proteinleri kendine çeker. Bu tezde üç ve beşinci karbonundan fosforlanmış $PI(3,5)P_2$ molekülü incelenmiştir. Bir otofaji proteini olan Atg18 proteinin koful üzerinde konumlanması $PI(3,5)P_2$ seviyeleriyle korelasyona sahiptir. Bu yüzden Atg18 proteininin kofula konumlanmasının, $PI(3,5)P_2$ lipidinin bir gösterge proteini olarak kullanılıp kullanılamaycağı sorgulanmıştır. Bu konumlanmayı sayıya dökmek için ImageJ-FIJI yazılımının EzColocalization adlı pluginden yararlanılmıştır. Bu plugin bize Pearson Korelasyon Katsayısı (PCC) denen bir değeri geri verir ve bu değer Atg18 proteinin kofula konumlanmasının büyüklüğünü ifade eder. $PI(3,5)P_2$ düzenleyici kompleksinin proteinlerinin, *VAC7*, *VAC14* ve *FAB1,* delesyonuna sahip hücreler ve ya sadece $PI(3,5)P_2$ lipidine bağlanan ya da hiçbir PIa bağlanmayan Atg18 mutantları incelenmiştir. Sayıya dökülmüş sonuçlar göstermiştir ki gerçekten de Atg18 proteinin koful üzerindeki konumlanması $PI(3,5)P_2$ seviyeleriyle artmıştır. Ek olarak Atg18 proteinin hücre döngüsü boyunca bir süre sadece yavru hücrenin kofuluna konumlandığı gözlenmiştir. EzColocalization plugini sayesinde bu gözlem matematiksel olarak gösterilebilmiştir. Birçok analizin sonucunda Atg18 proteinin yavru kofula özel konumlanması, koful segregasyounundan hemen sonra ve metafazdan sonra 5 dakika önce veya sonra başlayıp, anafazdan 5 dakika sonra kaybolduğu ve Atg18 proteinin ortalama 30 dakika yavru kofulda kaldığı gösterilmiştir. Orta log fazdaki popülasyonun %95'ten fazlasında Atg18 bir noktada yavru kofula özel konumlanırken, popülasyonun %49'unda koful segregasyonundan sitokineze kadar Atg18 proteini sadece yavruda konumlanmıştır.

PI(3,5)$P_2$ lipidinin regülatörlerinin de asimetrik konumlanma gösterip göstermediği incelenmiştir. Vac14 proteinin zaman atlamalı çekimlerinde, Vac14 proteinin herhangi bir kofula özel konumlanmadığı tespit edilmiştir. Yine orta log fazdaki popülasyonlarda anne ve yavru kofulunun floresans yoğunluğu ölçülerek yapılan analizlerde Vac7, Vac14, ve Fab1 proteinlerinde asimetrik konumlanma görülmemiştir. Öte yandan PI(3,5)$P_2$ metabolizmasıyla alakalı Sch9 ve Ivy1 olmak üzere iki protein daha incelenmiştir. Sch9 proteini anne kofulda güçsüz bir özgüllükle konumlanmıştır. Ivy1 ise güçlü bir özgüllükle yavru kofulda konumlanmıştır. Sadece PI(3,5)$P_2$ lipidine bağlanıp PI3P lipidine bağlanmayan Atg18 Sloop mutantı ise güçsüz bir özgüllükle yavru kofula konumlanmıştır. Bütün olarak, bu tezin bulgularo, Atg18 koful lokalizasyonunun PI(3,5)$P_2$ üretimim ile ilişkili olduğunu göstermekte ve böylece Atg18 proteinin PI(3,5)$P_2$ seviyelerinin gösterebileceğine iişaret etmektedir. Bununla beraber, anne ve yavru kofulun PI(3,5)$P_2$ fosfolpidine bağlanan bazı proteinler (Atg18, Sch9) ve PI(3,5)$P_2$ düzenleyicileri (Atg18 ve Ivy1) açısından farklı davranış sergilediğini göstermektedir.

# AKNOWLEDGEMENTS

I would like to thank TÜBİTAK (The Scientific and Technological Research Council of Turkey) for their funding and the opportunity they provided us to do science. (TÜBİTAK grant no: 219Z100).

I am quite grateful to my beloved PI, Asst. Dr. Ayşe Koca Çaydaşı. I have been working with her since 2018, and in our fifth year, our ways are separating. She is the best PI I have met so far in terms of being patient, understanding, and leading. I wish her much better people to work with and ease in her career.

I am also very thankful that my family always supported me both emotionally and financially. My mother, Ilknur, left her daily life in Aydın and moved in with me to support me for 2 years in a tiny flat. My father, Kadir, frequently visited us although we were miles apart. I appreciate this sacrifice a lot, and I wish them the best. My sister, Billur, kept her emotional support remote, I would wish her here by me more.

I owe the former graduate students of this too much. They were always responding to my silly questions and they took the time to show me the best way to conduct my studies. Plus, we were having too much fun before they graduated. We collected unforgettable memories, and moments together. I grew up with them, and now they are distributed all around the world. I hope our bond will never fade away. I want to give my special thanks to Dilara, Şeyma, Hüseyin, Betül, Barış, Cansu, and Idil.

Destiny made me meet with Mariam and I am very grateful. She came from Egypt and enlightened our lives with a bright light. Our discussions with or without red flags, mostly red flags, contributed to my character. She was the definition of being helpful and I don't know how I will pay her back. I wish her the best of the bests.

I want to thank Sevilay for going through all the hardness during a masters' period together.

Atakan Özcan came like a saviour to Koc and saved me with good company. Hemşerim, I will never forget you.

I want to thank my colleagues who were always supportive: Ceyda, Berfu, Dilşad, Büşra, Samet, and many other colleagues.

Angels, should I say, were the interns. They did all this lab maintenance work for us and contributed to my research by doing some of the work load. Ada, Sude, Doğa, and Eylül. This is my special thanks to you. I hope I could have taught you enough.

I want to express a great sincerity against Dr. Pınar Tatar Güner. She was always loving and caring to us since our undergrad years, and this continued for my grad years as well. Without her support, I would give wrong decisions. I am very grateful that I know her.

I want to thank Asst. Billur Çelebi Ergin. Working with her to have teaching experience was a lucky coincidence. I learned a lot from her teaching style. And she was always suggestive and supportive during my masters' period.

Finally, I would like to express my sincere gratitude to every professor and every friend I got to meet here at Koç University. In my opinion, Koç University is the best option in Turkey to do science. I hope it remains like that.

# TABLE OF CONTENTS

# LIST OF TABLES

# LIST OF FIGURES

# ABBREVIATIONS

| | |
|---|---|
| PI | Phosphatidylinositol |
| PI3P | Phosphatidylinositol 3 phosphate |
| $PI(3,5)P_2$ | Phosphatidylinositol 3 and 5 biphosphate |
| PCC | Pearson Correlation Coefficient |
| mNG | mNeongreen |
| PAS | Pre-autophagosomal Structure |
| Sloop | Scrambled Loop |
| MS | Mass Spectroscopy |
| PCR | Polymerase Chain Reaction |
| ORF | Open Reading Frame |
| OD | Optical Density |
| WT | Wild-type |
| SC | Synthetic Complete |
| TY | Tryptone – Yeast Extract |
| PDF | Probability Distribution Function |
| Fab1-HA | Fab1 - hyperactive |

# CHAPTER 1: INTRODUCTION

## *1.1 Phosphoinositides*

The cells majorly constitute of three molecule types: proteins, carbohydrates, and lipids. If I investigate those molecules by their charge, proteins are mostly amphipathic, carbohydrates are usually hydrophilic, and lipids are hydrophobic. Although there are three major classes, these molecules can undergo chemical modifications so that, for example, lipids can be amphipathic, too, by reacting with phosphate-bearing molecules. These lipids are called phospholipids and are the primary component of cell membranes and other organelle membranes. Being amphipathic, these lipids create a hydrophobic bubble in an aqueous medium where some proteins or lipids can anchor. The composition of the membranes is essential for vesicle or membrane structure, signaling, or trafficking. This thesis investigates one kind of phospholipid: phosphatidylinositol 3, 5 biphosphate ($PI3,5P_2$), a member of the phosphatidylinositol family. Inositol is a six-carbon ring that can be phosphorylated from the 3rd, 4th, and 5th through phosphodiester bonds between hydroxyl and phosphate groups (Balla, 2013). Our phospholipid of interest is phosphorylated from its third and fifth position of the inositol ring. This phosphoinositide is one of the least abundant in the cell, although it has essential roles in cell metabolism, such as autophagy (Balla, 2013).

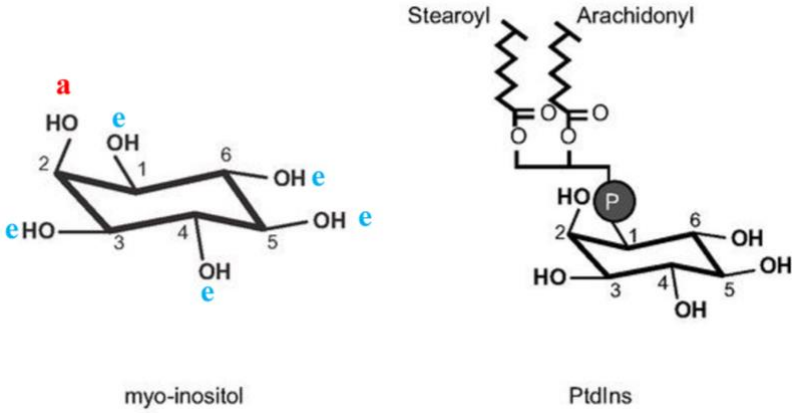


**Figure 1-1: The orientation of the OH-groups in myo-inositol**

The axial or equitoral positioning of the hydroxyls are represented in myo-inositols and PIs. There are 5 equitorial and 1 axial hydroxyl group and myo-inositol forms phosphodiester bond with lipids through its axial carbon. 3rd, 4th, and 5th, equatorial hydroxyl groups are phosphorylated differentially to form PIs. The image is adapted from (Balla, 2013).

## 1.2 Phosphatidylinositol 3,5- biphosphate ($PI3,5P_2$) Metabolism

PI(3,5)P2 synthesis starts with the synthesis of monophosphorylated inositol rings by kinases. Different kinases and phosphatases provide further modifications. In eukaryotes, it is synthesized by *FAB1* (PIKfyve is the mammalian ortholog) lipid kinase which phosphorylates PI3P from the fifth position. *FIG4*, on the other hand, codes for a lipid phosphatase which converts PI(3,5)P2 to PI3P. Although it is expected to increase, PI(3,5)P2 levels decrease upon deletion of FIG4 that means Fig4 functions not only as phosphatase in the metabolism of PI(3,5)P2 (Hasegawa et al., 2017). . This suggests that Fig4 is required for Fab1 activity as well.

The axial or equatorial positioning of the hydroxyls can be represented with Agranoff's turtle. (Balla, 2013)

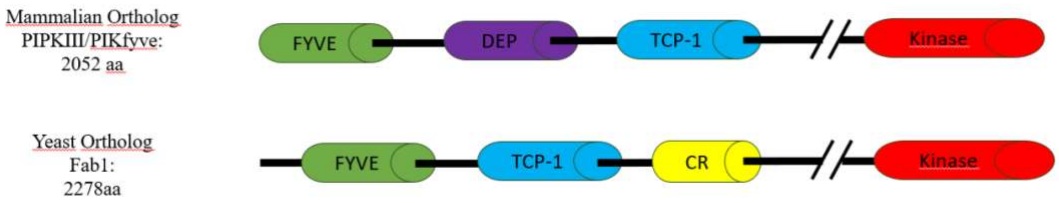


**Figure 1-2:The domains of Fab1 and its ortholog PIKfyve in mammalian**

PIKfyve is human ortholog of Fab1 in yeast. In this figure, the domain homology is investigated. FYVE is pH dependent transmembrane protein that binds PIs, DEP takes place in G-protein signalling pathways, TCP-1 is cytosolic equivalent of groEL, and Kinase domain phosphorylates PIs. This image is adapted (Balla, 2013).

$PI(3,5)P_2$ is regulated by a complex called $PI(3,5)P_2$ regulatory. The proteins that constitute the complex are Vac14, Fab1, Fig4, Atg18, and Vac7 in budding yeast. Vac14 is a large protein and acts as a scaffold protein for the other members of the regulatory complex (Schulze et al., 2014).Vac7 only exists in yeast, although there are candidates for being ortholog of Vac7 due to their similar LEA-2 domains, which is a lipid transport domain, with Vac7. These candidates are TMEM106B, and Tag1C (Levine, 2022). Vac7 in yeast has a transmembrane domain and tethers Vac14 and the proteins that are bound it to vacuole membrane increasing the stability of the regulatory complex (Gary et al., 2002). Fab1, as aforementioned, is a lipid kinase that

converts PI3P to PI(3,5)$P_2$ while Fig4 is doing the vice versa. This suggests that Fig4 is required for Fab1 activity as well. Fig4 mutants that have defective catalytic sites, reduced the activity of Fab1. This is explained by conformational change of Vac14, allowing Fab1 to either bind to or stay away from the vacuole membrane (Strunk et al., 2020). Reduced levels of PI(3,5)$P_2$ causes vacuoles to swell and increase its pH (Gary et al., 1998).This phenotype is seen in Vac7 and Vac14 deleted strains. The reason for this may be that PI(3,5)$P_2$ is required for $H^+$ pump V-ATPase, Vph1, assembly on the vacuole membrane (Banerjee & Kane, 2020).

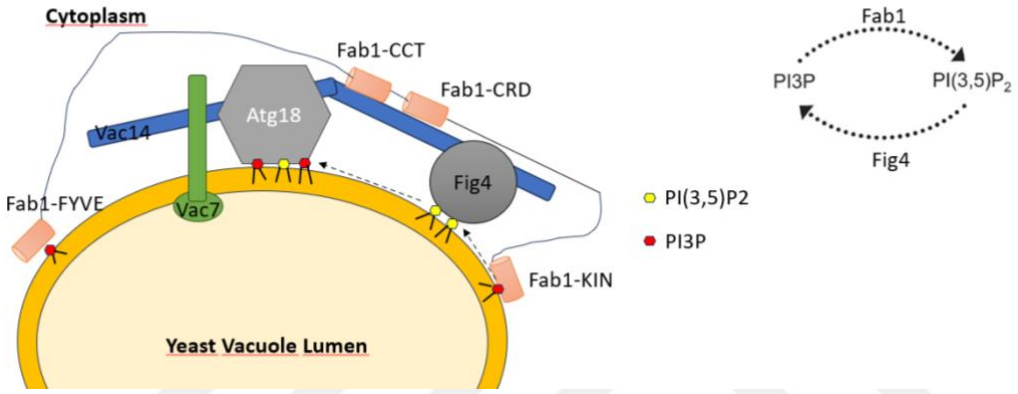


**Figure 1-3: PI(3,5)P2 regulatory complex**

This figure represents PI(3,5)P2 regulatory complex proteins.Vac14 acts as scaffold, Vac7 has transmembrane domain, Fab1 phospharylates PI3P, Fig4 removes phosphate from PI(3,5)$P_2$, Atg18 is bound to both PIs. The picture is adapted from (McCartney et al., 2014)

Yeast vacuoles function similar with mammalian late endosome and lysosomes. They are acidic and proteins carried inside undergoes hydrolysis. Lysosomes are an important component of autophagy since it is the final destination for proteins which are determined to be degraded. In a work where autophagy related proteins were sought, multiple proteins were found to form a complex in nutrient-rich or starvation conditions in yeast cells; then this complex was called pre-autophagosomal structure (PAS) and the proteins constituting this structure is called Atg proteins (Harding et al., 1996; Klionsky et al., 2003; Takeshige et al., 1992). A particular Atg protein is important for this research: Atg18. This is because it is also a member of PI(3,5)$P_2$ regulatory complex. As a PAS member it binds to Atg2 and recruits other PAS members by starting the formation of isolation membrane. Atg18 binds to PI(3,5)$P_2$, as previously mentioned, and PI3P. This Atg18-Atg2 complex is responsible for formation of isolation

structure. Atg18 binding to vacuole, Atg2 binding to ER and PAS complex provides isolation structure a ground to enlarge (Kotani et al., 2018). The proteins recruited by $PI(3,5)P_2$ eventually regulate vacuole morphology, and characteristics, and Atg18, being one of them, has functions other than autophagy in yeast cells. Atg18 negatively effects Fab1 function by interacting with Vac7 (Efe et al., 2007). $PI(3,5)P_2$ levels are elevated in *atg18Δ* by either hyperosmotic shock or fab1-ha, the swollen vacuole phenotype is not rescued, suggesting that Atg18 inhibits Fab1 activity by elevating $PI(3,5)P_2$ levels (Efe et al., 2007). Atg18 was used as a marker for $PI(3,5)P_2$ previously, and it was known that it binds both PI3P and $PI(3,5)P_2$ and as soon as it localizes to vacuole membrane α-helices in its structure embeds in the vacuole membrane which leads to membrane scission and tubulation (Gopaldass et al., 2017). In order to be able to work with either only-$PI(3,5)P_2$ binding Atg18, or an Atg18 variant which cannot bind any phosphoinositide, certain mutations were introduced to the Atg18. PI3P binding domain of Atg18 is scrambled (Atg18-Sloop), or two glycine was added between 285$^{th}$ and 286$^{th}$ amino acids on Atg18 (Atg18-FGGG) (Gopaldass et al., 2017). These mutants were exploited in our experiment frequently.

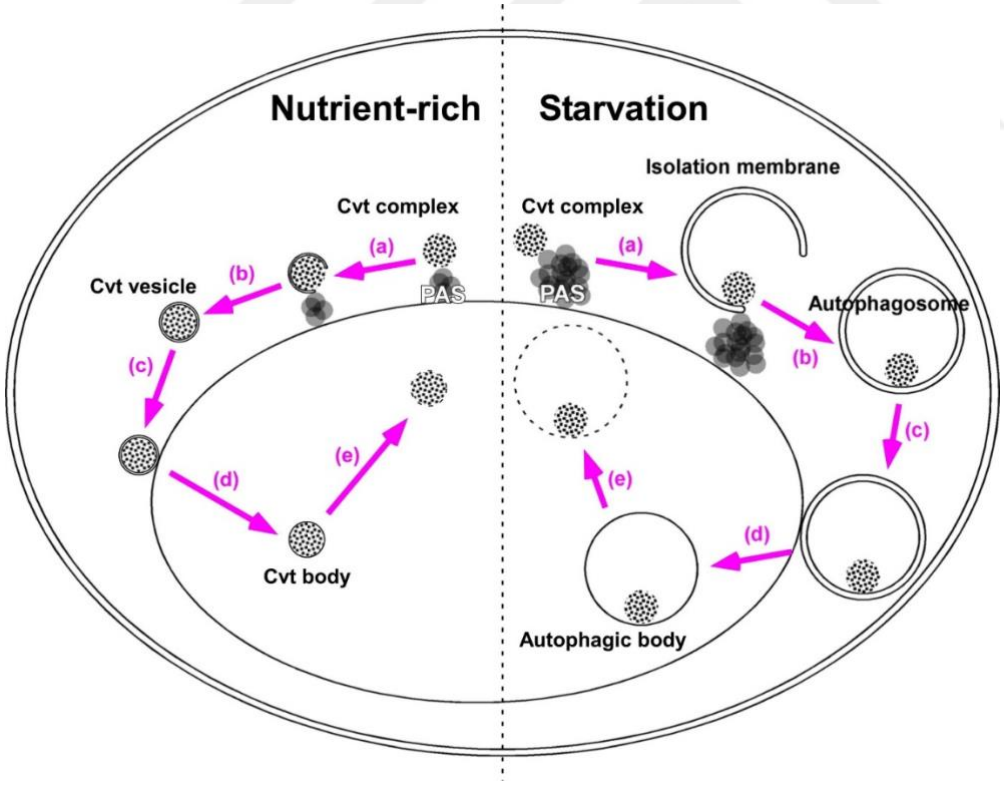


**Figure 1-4:PAS complex activity under nutrient rich and starved conditions**

This figure depicts how PAS complex rule autophagy in nutrient-rich and starvation conditions. In nutrient rich conditions, material that is going to be degraded is surrounded by Cvt vesicle; however, in starvation conditions it is taken in a autophagosome. This image is taken from (Suzuki & Ohsumi, 2010).

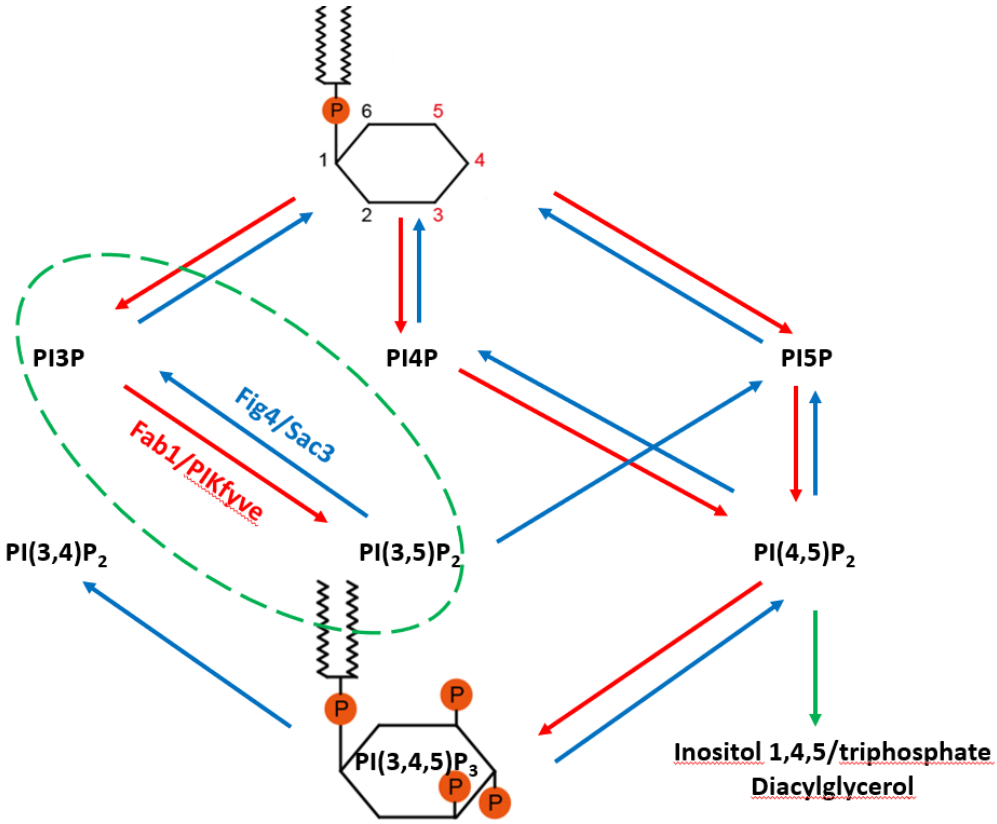


**Figure 1-5:Interconversion of phosphoinositide species**

Our research focuses on the selected reaction. Phosphate on the fifth position of PI(3,5)$P_2$ is removed by Fig4 and OH group on the fifth position of PI3P is phosphorylated by Fab1. This image is adapted from (Hasegawa et al., 2017).

## *1.3 Phosphatidylinositol 3,5- biphosphate (PI3,5$P_2$) Functions*

Despite phosphoinositols are found throughout the whole membranous system of the cell, PI(3,5)$P_2$ specifically localizes on the outer membrane of late-endosomes and lysosomes of mammalian cells, and on the vacuoles of yeast cells. Being localized there provides us with a hint that this PI has a role in autophagy. Indeed, PI(3,5)$P_2$ regulates induction, closure & fusion, and degradation steps of autophagy (Palamiuc et al., 2020). These steps are shown in figure 6. Apart from having a function in autophagy, PI(3,5)$P_2$ levels correlate with the increased saline concentration. The amount of PI(3,5)$P_2$ increases within the 10 minutes after 0.9M NaCl introduction and the levels go down to basal levels in 30 minutes after introduction of hyperosmotic environment (Dove et al., 1997). Plus, the vacuole size decreases as vacuole numbers increases upon hyperosmotic shock. This event increases surface to volume ratio of

vacuoles (Bonangelino et al., 2002). This phenomenon may suggest that PI(3,5)$P_2$ may serve as a protection by regulating vacuolar fission. PI(3,5)$P_2$ not only gives response to saline concentration, but also to nutrient levels since it was shown that it interacts with mTORC in mammalian cells (Posor et al., 2022). PI(3,5)$P_2$ promotes endocytosis upon lack of nutrients (Wallroth & Haucke, 2018). This nutrient sensing capacity and autophagy aspects work synergistically. PI(3,5)$P_2$ also take role in regulation of V-ATPases, for example Vph1p, which are proton pumps. Therefore, it can also be said that PI(3,5)P2 is responsible for pH balance of the vacuole in baker's yeast (Banerjee et al., 2019; Li et al., 2014). The role of PI(3,5)$P_2$ in osmoregulation is not a surprise knowing that its levels increase open hyperosmotic shock. In one of the studies it was shown that depleted PI(3,5)$P_2$ increases the potassium cation concentration in the vacuoles of baker's yeast (Wilson et al., 2018). Additionally, PI(3,5)$P_2$ can talk to $Ca^{2+}$release pathways by interacting with TRPLM and regulate membrane fusion-fission events (Dong et al., 2010).

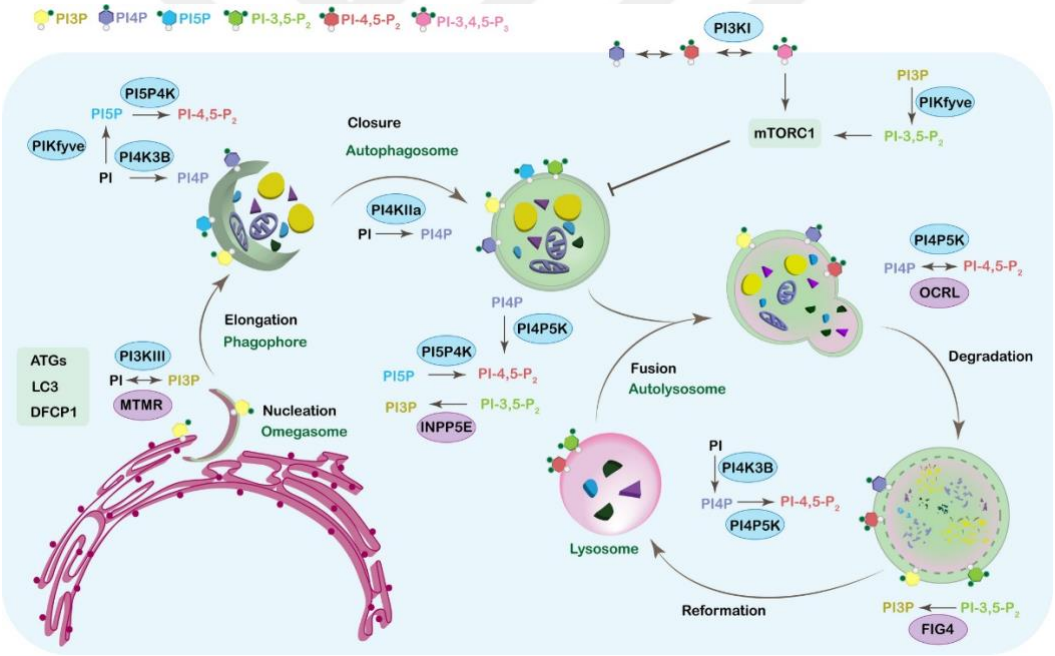


**Figure 1-6:The role of PIs in autophagy.**

PI(3,5)$P_2$ converts late endosomes to lysosome in mammalian cells interacting with mTORC pathway. This image is taken from (Palamiuc et al., 2020).

Playing a role in autophagy and lysosome chemistry, PI(3,5)$P_2$ is crucial for human health affecting the health of neurons or other systems. The lack, or dysfunction of phosphatases that regulate PI(3,5)$P_2$ may cause several diseases. FIG4 dysfunction causes Yunis–Varon-syndrome, amyotrophic and primary lateral sclerosis. FIG4, MTMR2, MTMR5 (SBF1),

MTMR13 (SBF2) dysfunction causes Charcot–Marie–Tooth disease of several types. MTM1 dysfunction causes X-linked centronuclear myopathy. MTMR14 dysfunction causes Centronuclear myopathy (Posor et al., 2022). Dysfunctional kinases that form $PI(3,5)P_2$ cause diseases as well. PIPK3 dysfunction causes Fleck corneal dystrophy (Posor et al., 2022).

## *1.4 Saccharomyces cerevisiae*

### *1.4.1 As a Model Organism*

*Saccharomyces cerevisiae* is a unicellular eukaryotic cell which belongs to the kingdom of Fungi. It can be found in either haploid or diploid form. Haploid yeasts can mate and form 2n yeasts, diploid yeasts can sporulate and form n yeasts. There are two types of spores in yeast, MATa and MATalpha. Further information is given in the "Its cell cycle" section. Knock-out experiments and libraries are ideal for haploid spores since we only need to worry about one allele. Being able to mate, we can screen genetic interaction of two different genes. They grow by budding and one life cycle of wild-type yeast is about 1.5 to 2 hours. Baker's yeast grows at 30°C and they can grow in comparably cheap media. These factors result in quick and cheap experiments. Although they grow slower than *E. coli*, they still grow fast, and they are eukaryotic which means yeasts share much more molecular systems with mammalians than bacteria. There is a high degree of conservation between yeast and mammalian cells in the following molecular processes: autophagy, protein translocation and secretion etc. Genetically 47% of 414 essential genes are replaceable in one to one ratio with human orthologs (Nielsen, 2019). *S. cerevisiae* is the first eukaryote whose genome was firstly sequenced. The hopes of baker's yeast being available as a model organism went up once h-Ras human ortholog was reintroduced to the *RAS1 RAS2* deleted yeast strains. Yeasts bearing this double deletion were inviable; however, reintroduction rendered yeasts viable again (Botstein et al., 1997).
In conclusion, baker's yeast *Saccharomyces cerevisiae* is a brilliant model organism in order to study conserved mechanism in eukaryotes.

### *1.4.2 Its Cell Cycle*

After cytokinesis, daughter cell snips from the mother cell and becomes an independent yeast cell (Hartwell & Unger, 1977). The most generic definition of cell cycle would be that it is the period where cells get ready for division and divide into two cells. Cell cycle consists of two parts interphase and mitosis (Alberts et al., 2002). Interphase is the phase where the cell gets

ready for division, and the mitosis, or meiosis, is the stage where cells undergo division. There are three phases in interphase: G1, S, and G2. In G1 phase the cells get large enough to be able to divide, in S phase genetic material is duplicated, and in G2 phase, again, the cell checks nutrient availability. Once the cell pass from G1 to S (G1/S transition) cell becomes committed to divide (Alberts et al., 2002). At the G1/S transition, Baker's yeast starts budding. Buds, so called daughter cells, emerge from the mother cell and all the needed materials are transported to the daughter cell during the cell cycle. Baker's yeast is also called budding yeast referring to its division that occurs through budding. In mitosis (M phase) duplicated genetic material is segregated to the mother and daughter cells. For this, first, duplicated DNA condenses to form condensed chromosomes composed of two sister chromatids. Then, condensed chromosomes align in the metaphase plate and sister chromatids separate and segregate to the opposing poles of the cells. This way, each cell gets one exact copy of the genomic material. During M-phase, other organelles such as vacuoles migrate to daughter cell as well. The mitosis that yeast cells undergo is called closed mitosis referring the undissolved nuclear membrane through mitosis. M-phase is followed by cytokinesis, where the cells physically separate (Alberts et al., 2002).

Fidelity of the cell cycle is assured via checkpoints. If there is a mistake with crucial steps such as genome duplication, cell cycle halts until the mistake is corrected. When the cell cycle halts, cells stop moving to other phases and such cells are called arrested cells. Arrested cells are used to depict some protein works in that checkpoint or synchronize the population so that every cell in the population is in the cell cycle phase (Morgan & New Science, 2007) . The most common checkpoints are cell size control, DNA damage responses, monitoring DNA replication, S-M dependency, and the mitotic spindle checkpoint (Barnum & O'Connell, 2014). Checkpoints working along with cell cycle mechanisms ensure a healthy daughter cell; therefore genomic-wise stable progenies.

One more advantage of working with budding yeast except the one mentioned in the previous section is that one can define in which cell cycle phase is a yeast cell by looking at its morphology. In G1 phase, the mother cell has "no bud", yet the bud-site is determined. In S phase, bud is emerging, but it is quite tiny. The bud grows in G2 phase, but it is not as large as the mother cell. Through the end of mitosis, before cytokinesis, the daughter grows as large as the mother cell in wild type yeast (Byers & Goetsch, 1974).

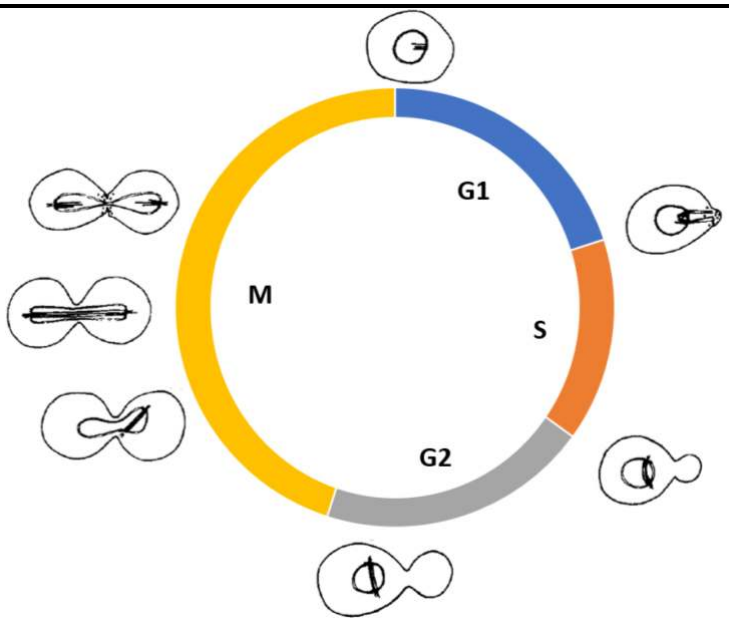


**Figure 1-7:Stages in the mitotic cycle in haploid *Saccharomyces cerevisiae.***

This figure depicts spindles, nucleus membrane and cell membrane structure along with bud formation throughout the cell cycle. This figure is adapted from (Byers & Goetsch, 1974)

### *1.4.3 Vacuole Segregation*

Vacuoles regulate pH, act as a lysosome, sense nutrient deprivation, and maintain cation concentration. In budding yeast, vacuole inheritance starts in the beginning of the cell cycle and finalizes in G2 before nucleus moves into daughter cell (Weisman, 2003). During the inheritance of vacuole, vesicle pitching out from the vacuole moves back and forth on a tubular actin structure by Myo2 motor protein (Weisman et al., 1987). In yeast mutants where the vacuole cannot be inherited, it was shown that fresh vacuole is generated in the bud so that cell cycle can progress (Raymond et al., 1990; Weisman et al., 1987). Inheritance of the mother vacuole in bud is limited with 50%, and the rest of the vacuole is generated (Lois S. Weisman, 2003). In a screening where allow us to see vacuole defects (vacuoles are essential, yeasts bearing no vacuoles are inviable) four classes of vac proteins were characterized based on the size of the vacuoles. In this screening, particularly important for this thesis, class III non Vps mutants presented significantly large vacuoles with defects in trafficking. Those genes were *FAB1*, *VAC7*, *VAC14*, and *FIG4*, later they will be called as PI(3,5)$P_2$ regulatory complex. As discussed earlier (in section xx) these proteins regulate PI(3,5)$P_2$ synthesis. Myo2 is the motor protein that carries maternal vacuole to the daughter cell along actin cables (L. S. Weisman,

2003). Myo2 motor protein recognizes vacuoles by interacting with Vac17 (Tang et al., 2003). However, Vac17 has no transmembrane domain. This Vac17 – Myo2 complex is tethered to vacuole by Vac8, which has a transmembrane domain, interaction (Tang et al., 2006).

Vac17 has a PEST sequence which allows it to be degraded. Vac17 without PEST sequence accumulates on the daughter vacuole, and in the vacuole inheritance mutants that have wild-type Vac17, Vac17 is accumulated in the mother vacuole. These suggest that Vac17 has a daughter-specific turnover (Tang et al., 2003). When Vac17 is stabilized with its PEST deleted, Myo2 remains bound to vacuole. Since Myo2 does not release the vacuole, the vacuole can be carried back to mother. Therefore, it can be said that, Vac17 turnover is important for unidirectional migration of vacuoles to the daughter cell (Ishikawa et al., 2003).

Vac8 has, at least, three functions depending on with which protein it interacts. Vac8 binding Vac17 functions at vacuole inheritance, as already mentioned. Vac8 binds two more proteins: Nvj1, and Apg13. Nvj1 interaction is required for nuclear-vacuole junction (Pan et al., 2000), and Apg13 interaction is required for autophagy and cytoplasm to vacuole targeting (Scott et al., 2000).

Further experiments showed that Vps21 and its interaction partners may be responsible for Myo2p attachment to the segregation structure which is a name for the inheriting vacuole (Horazdovsky et al., 1994; Singer-Krüger et al., 1995).

Interconversion of PI3P and PI(3,5)$P_2$ may be responsible for spatial and temporal control of vacuoles during segregation considering there are proteins specifically recruited by PI3P, or PI(3,5)$P_2$, and commonly by both of these phosphatidylinositols (Gary et al., 2002; Sbrissa et al., 2002; Vicinanza et al., 2008; Wishart et al., 2001; Wurmser & Emr, 2002).

# AIM OF THE THESIS

There are two aims of this thesis. The first one is finding a way to quantify localization, and the second one is unraveling the mechanism behind Atg18 localization on daughter vacuole only during cell cycle. For quantization of localization PCC scores are exploited. For asymmetric localization, FI measurement and PCC scores are utilized.

# Chapter 2: MATERIALS AND METHODS

## *2.1 Saccharomyces cerevisiae Methods*

The recipes of reagents, media, and buffers are denoted in the Table 2, Appendices.

### *2.1.1 Yeast Strains and Plasmids*

Yeast strains were constructed through recombination with PCR based cassettes or linearized plasmids or through introduction of circular plasmids to the S288C background and its derivatives. PCR-based cassettes were used in order to do endogenic DNA manipulation, such as gene deletion or insertion into 5' or 3' of the ORF for tagging from either side of the protein. Plasmid introduction was used so that the plasmid can be gotten rid of with proper conditions; therefore, we were able to observe essential gene malfunctions. The "Colony PCR" method was applied to confirm gene deletions (See PCR methods). The tagged proteins were confirmed either with microscopy (See Microscopy methods) or western blot depending on the tag. If the tag was a fluorophore, we confirmed by microscopy. Epitope tagging with HA or Myc, were confirmed via western blot. The strains and plasmids used in this thesis are listed in tables 3 and 5 in the Appendices.

### *2.1.2 Yeast Growth*

Yeasts were grown at 30°C. Cells were grown in YPAD liquid media in a shaking incubator at 160 rpm or on YPD agar plates in a steady incubator unless otherwise stated. The amount of liquid media used in a certain flask was determined with 1:5 ratio. For example, 10ml liquid culture is grown in 50ml Erlenmeyer Flask. To obtain log-phase culture: first cells taken from agar plates were inoculated into liquid media and grown overnight to receive a stationary culture. Next morning, the optical density (OD) ($1OD_{600}$ equals to $2.2*10^7$ cells/ml) of the culture was measured with a spectrophotometer (PG Instrument, T60 Visible Spectrophotometer) at 600 nm. Then, the overnight culture was diluted to 0.15 $OD_{(600)}$ with fresh media and incubated further to reach at least 0.8 $OD_{(600)}$ to obtain a log-phase culture. This log-phase culture can be kept in log-phase by diluting the cells to prevent their $OD_{(600)}$ reaching beyond 1 $OD_{(600)}$. For timelapses, the culture was kept at log phase for at least 24h. In order to do that, there was an extra step added after getting 0.8 $OD_{(600)}$: diluting so that there

is a 0.5 $OD_{(600)}$ culture the next morning. To calculate that, 1.5 h duplication time was assumed for wildtype, or strains bear no deletion, and more time was assumed for deletions. It was done so that I have a culture remained at log phase for 24 hours, and the timelapse protocol can be initiated directly in the morning. The cultures that will be investigated with microscopy were grown in filter-sterilized SC-Comp media to avoid background signals.

### *2.1.3 Competent Cell Preparation*

To make competent cells, 50ml log-phase culture was taken to a 50ml falcon, cells were precipitated at 3200 rpm for 2 minutes, and the supernatant was discarded to liquid waste by decantation. The pellet was washed with sterilized $ddH_2O$ and precipitated with the same conditions. Then, the pellet was washed with 25ml LiSORB. The suspension in LiSORB was precipitated with the same conditions, and excess LiSORB on the pellet was aspirated. For 1 OD of cells, 300µl LiSORB, and 50µl of denatured Salmon Sperm DNA were added to the pellet. If OD was less, the LiSORB and Salmon Sperm amounts were downgraded with the same ratio. To obtain denatured Salmon Sperm DNA, Salmon Sperm DNA was thawed, kept at 95°C for 5 minutes in advance. The pellet was resuspended in the LiSORB added and aliquoted to 1.5 ml Eppendorf tubes with 100µl volumes. The aliquots were kept in -80°C until being used.

### *2.1.4 Transformation*

Yeast competent cells were thawed at room temperature. 5µl of cassette PCR product, or 1-2µl of plasmid of interest, were added to the competent cells as 50µl of competent cell vial was left aside to have a negative control. After 15 minutes of incubation. 300µl of LiPEG was added to all competent cell vials and vigorously vortexed. The cells were incubated at room temperature for 20 minutes. 35µl of DMSO was added to all the vials, vigorously vortexed. The vials were taken to a 42°C water bath and incubated for 15 minutes. Later, the transformation suspension was taken to centrifuge at 3200 rpm for 2 minutes. The supernatant was aspirated. Transformants were selected by auxotrophy or antibiotic resistance depending on the selection marker present on the cassette or introduced plasmids. If the selection marker was an auxotrophy marker, then the pellet was suspended with 200µl 1X PBS, and the suspension was plated out on the regarding solid agar media. If the selection marker was antibiotic sensitivity, then the pellet was suspended with 1ml YPAD, and this suspension was added to 2ml YPAD in a test tube. The 3ml media containing transformed cells were incubated at 23 overnight. The

next morning, 3ml culture was precipitated, the pellet was suspended with 150µl 1X PBS and plated out on the regarding solid antibiotic plate. Thereby, the cells were allowed to produce resistance genes before being exposed to the antibiotic. Cell suspensions were plated out by pipetting the suspension in the middle of the solid agar plate and adding glass beads. The glass beads were shaken so that the suspension of transformed cells is spread equally throughout the solid agar plate. After the plates dried, the glass beads were removed, and the solid agar plates were incubated at appropriate temperature. After two days, colonies were selected with sterilized toothpicks and streaked on another sectored plate to obtain single colonies coming from the same clone. Two days later single colonies were picked and streaked as patches to obtain more cells coming from the same clone. In two days, these patches grew, and after they were confirmed as aforementioned, cells were scraped from the agar and frozen in 15% glycerol at -80°C and placed into the collection.

## *2.2 PCR-based Methods*

### *2.2.1 Cassette PCR*

The double-stranded DNA fragments with complementation to the gene of interest, selection marker, and-or tags are called cassettes. Complementation to the gene of interest was provided when the primers (S1, S2, S3, S4) were designed. S1 and S2 primers were used for deletion, and S2-S3 were for C-terminal tagging. The S- primers were complementary to the plasmids in our collection and to the gene of interest from their overhangs. Selection marker and tag sequence were provided from the plasmid. The cassette PCR reaction was usually 50 µl. There were 5 µl of 20ng/µl template plasmid, 3.2 µl forward (10µM), 3.2 µl reverse (10µM), 5µl 10X PCR Buffer 1 (homemade), 8.75 µl 2mM dNTPs (NEB #N0446S), 0.6µl Taq-VENT polymerase mix (2X Taq Polymerase (NEB #M0273L) and 1X VENT Polymerase (2U/µl, NEB#M0254S), and 24.25µl dd$H_2O$ inside the cassette PCR reaction. The reaction was run in a thermocycler (Biometra Tadvenced Twin Analytik Jena PCR machine) with the following conditions: 2 min at 95°C (1), 30 sec at 95°C (2), 30 sec at 52°C (3), X min at 68°C (4), 30 sec at 95°C (5), 30 sec at 52°C (6), X min with an increment of 20 sec per step at 68°C (7), forever at 4°C (8). Steps from 2 to 4 were cycled nine times, and steps from 5 to 7 were cycled nineteen times. X was a time variant that depends on the size of the PCR product. 1 min per 1kb ratio was used to calculate X. 0.8% Agarose Gel Electrophoresis technique was used to see if cassettes are amplified at the desired size.

### *2.2.2 Yeast Colony PCR*

In order to confirm deletions, different primers that either bind in front and at the end of the gene or in front and the middle of the gene were utilized. The former was called external genotyping, and the latter was internal genotyping. In order to be able to use the genomic DNA of the transformants, the cells were lysed with a specific lysis buffer (0.01% Sarkosyl in 0.02M NaOH). The cells were lysed in 50µl lysis buffer by being heat-treated at 95°C for 15 minutes. The PCR reaction for one patch contained the following ingredients: 1.25µl of 10µM forward and reverse primer, 2.5µl of 10X Buffer 2 (homemade), 2.5µl of 2mM dNTPs, 0.3µl of Taq Polymerase (5U/µl), 1µl of lysed patch supernatant, and 16.2µl of dd$H_2O$. PCR thermocycling variables were as following: 5 min at 95°C (1), 30 sec at 95°C (2), 30 sec at 54°C (3), X min at 68°C (4), 3 min at 68°C (5). Steps from two to four were repeated for 35 times. 1 min per 1kb ratio was used to calculate X. 0.8% Agarose Gel Electrophoresis technique was used to see if cassettes are amplified at the desired size.

### *2.2.3 Plasmid isolation from E. coli*

Plasmids were isolated manually using alkaline-lysis and alcohol precipitation method. *E. coli* strain bearing a plasmid of interest was taken out to an appropriate TY plate. When bacteria grew, a single colony was inoculated in 3ml of appropriate TY liquid media overnight (18h) at 37°C. At room temperature, 2ml of overnight culture was precipitated at 6000 rpm for 5 minutes. The supernatant was aspirated. Homemade buffers that are called P1, P2, and P3 were used in the following step. 300µl P1 was added to the pellet and the mixture was vortexed vigorously. Later, 300µl P2 was added to the mixture, and it is mixed by inversion-rotation. Right after mixing, 300µl P3 buffer was added, and it was remixed by inversion-rotation. The mixture was centrifuged at 14000rpm for 10 minutes so that cell debris and other insoluble contaminants precipitate. After centrifugation, the supernatant was pipetted into a fresh Eppendorf tube, including 500µl isopropanol (ACS #0312.2500). The mixture was inverted-rotated again and then placed into the centrifuge at 14000 rpm for 20 minutes. The supernatant was discarded, and on top of the invisible pellet of isolated DNA 500µl 70% ethanol was added. The mixture was re-centrifuged with the same conditions as before. Ethanol was aspirated, and the pellet was re-centrifuged. Eppendorf tubes were then placed in a 65°C heat block until all the ethanol was evaporated. After, the pellet was dried, the invisible pellet was dissolved in 30µl water. The concentration and the purity of the plasmid isolated were measured with

NanoDrop. The remaining plasmid was stored at -20°C. The list of plasmids used in this study are shown in Appendices, Table 5.

### *2.2.4 Site-directed Mutagenesis*

pFA6a-mNeonGreen-KanMX plasmid was modified through site-directed mutagenesis to be able to bind S2 and S3 primers. This step was repeated twice with different pair of primers. Second mutagenesis was done to have the linker sequence in-frame with the gene and mNeongreen. The first set of primers were NeongreenS3linker-fw and NeongreenS3-linker-rev. The second set of primers are NeonGreenPntMUT2-FW and NeonGreenPntMUT2-Rev .The confirmation of mutagenesis was done by sequencing. The primer used for sequencing was SeqForNeongreen . The recipe of 50µl PCR reaction was as follows: 5µl PFU buffer, 1.5µl PFU polymerase, 5µl 5ng/µl plasmid, 4µl 2.5mM dNTP, 1.5µl forward primer, 1.5 µl reverse primer, and 31,5 µl dd$H_2O$. The recipe of the 50µl negative control reaction was as follows: 5µl PFU buffer, 5µl 5ng/µl plasmid, and 31,5µl dd$H_2O$. The sequences of the primers were given in Appendices Table 4.

### *2.2.5 Subcloning*

After site directed mutagenesis of pFA6a-mNeonGreen-KanMX, the resultant plasmid was called pMUK002. pMUK002 had served as a backbone whereas inserts, selection markers, came from different plasmids from the laboratory's collection. For his auxotrophy pFA6a-*HISMX6*, for hygromycin-resistance pKS133, and for natrunculin-resistance pKS134 plasmids were used. 8µg of plasmid was used for each double digestion. Restricted plasmids, later, were run in 0.8% gel electrophoresis, and inserts and backbones were extracted with gel extraction protocol. Extracted inserts and backbones were ligated respectively with the ligation protocol. The confirmed plasmids were amplified with *E.coli* transformation and miniprep.

#### *2.2.5.1 Restriction*

Double digestion was run with the following conditions: Plasmid equivalent of 8µg, EcoRV 1µl, BglII 1µl, 10X Tango Buffer 20µl, and enough dd$H_2O$ complementing to 100 µl reaction volume. The reaction was incubated at 37°C for 3 hours.

#### *2.2.5.2 Gel Extraction*

The kit from Machere-Nagel (MN) named "Nucleospin® PCR clean-up and Gel extraction" was used.

*2.2.5.3 Ligation*

For ligation reaction following reagents were used as following: 2 µl Backbone, 1 µl T4 Buffer, 0.5 µl T4 ligase, the amount of $ddH_2O$ and insert used is indicated in the Table 1. The reaction is incubated at room temperature for 30 minutes.

**Table 1: This table indicates the amount of insert and water used in ligation reaction.**

| Inserts | Insert from pFA6a-HISMX6 | Insert from pKS133 | Insert from pKS134 | Negative Control |
|---|---|---|---|---|
| Insert Volume | 6.5 µl | 4 µl | 5 µl | 0 µl |
| $ddH_2O$ Volume | 0 µl | 2.5 µl | 1.5 µl | 6.5 µl |

*2.2.5.4 E. coli transformation*

10 µl of ligation product was added to 100 µl dH5α *E. coli* competent cell. One 100 µl competent cell was remained without any DNA to be used as a negative control. The DNA and competent cell mixture was incubated on ice for 30 min. After being on ice, the reactions were transferred to a 42°C water bath. There, the reactions were incubated for 90 seconds. Right after 90 seconds, the reaction was incubated on ice for at least 5 minutes. The cells were plated out to a TY agar plate with a regarding antibiotic. They grew at 37°C. The plasmids were isolated via Miniprep.

## *2.3 Microscopic Analysis*

### *2.3.1 Live Cell Imaging*

All the images were taken using Carl ZEISS Axio Observer 7 motorized inverted epifluorescence microscope equipped with Colibri 7 LED light source, Axiocam 702 Monochrome camera, 100X and 63X Plan Apochromat immersion oil objective lenses, Filter sets 95 (GFP/Cherry), 20 (Rhodamin), FITC and DAPI and an XL incubation and climate chamber. Cultures for microscopy were prepared in SC-complete filter sterilized media.

*2.3.1.1 Still Images*

1 ml of log-phase culture (defined in yeast methods) was precipitated at 3200 rpm for 2 minutes. The pellet was resuspended in either SC-Comp filter sterilized or 0.9M NaCl SC-Comp filter sterilized media. Microscopy settings were 2x2 binning, mCherry exposure 500ms, FITC exposure 492ms. 63X objective lens with immersion oil is used in all experiments.

#### *3.3.1.2 Timelapses*

24h-log-phase (defined in yeast methods) at 0.5 $OD_{600}$ was used. First 150 µl of 6% Concanavalin A *(Canavalia ensiformis* Jack Bean, type IV Sigma C2010-G) was pipetted on the glass circle at the bottom of petri dish. (WVR 10810-054 Matsunami). After 10 minutes, Concanavalin A was pipetted back to Eppendorf and the glass-bottomed petri dish was washed with autoclave sterilized double distilled water five times. 200 µl of 24h-log-phase culture was pipetted on the glass bottom and the petri dish was taken to 30°C incubator for 30 minutes. After 30 minutes, petri dish was washed five times with 30°C filter sterilized SC-Comp. After the last washing, some SC-comp was left up to half of the petri dish. Then, the petri dish was taken into pre-heated (30°C) microscope climate temperature and there it was incubated for 1h in order to reach equilibrium between environment and petri dish at 30°C. At the end of the 1h time-lapse had been started.

### *2.3.2 Image Analysis*

#### *2.3.2.1 Fluorescence-based Manual Analysis*

Fluorescence intensity was measured with a software called imageJ – FIJI. The average intensity of 2x2 squares were measured and used in the ratios shown in the results. The d/m ratio simply means $\frac{d[(g_v-g_{bg})/(r_v-r_{bg})]}{m[(g_v-g_{bg})/(r_v-r_{bg})]}$; where m is mother, d is daughter, $g_v$ is mNeongreen through FITC fluorescence intensity on vacuole, $g_{bg}$ is mNeongreen through FITC fluorescence intensity on cytosol (background), $r_v$ is mCherry through mCherry fluorescence intensity on vacuole, $r_{bg}$ is mCherry through mCherry fluorescence intensity on cytosol (background).

#### *2.3.2.2 ImageJ-fiji macro Ez-Colocalization*

EzColocalization was downloaded from the given web source: https://sites.imagej.net/EzColocalization/plugins/. Reporter 1 was picked to be mCherry, and reporter 2 FITC. Cell identification input was ROI manager. For this plugin to work, Analyze → Set Scale → choose "Global", setting must be done. For analysis Threshold: PCC must be chosen along with for cell identification input ROI(s). Each vacuole was chosen with "oval" tool and each selection was saved as ROI. When "analyze" button is clicked, the software merges overlapping oval shapes and makes them into one cell# value. In the results list, there is a Pearson coefficient value corresponding to cell#. Pearson coefficient is a mathematical value which represents colocalization and it has a value between 1 to -1. Values closer to 1

means colocalization, 0 means complete randomness, and -1 means the two reporters push each other away.

### *2.3.3 Statistical Analysis:*

Statistical analyses were done with the software called Prism 8.0.1 (GraphPad, La Jolla, CA). One-way Anova, and unpaired t-test were used to determine the significance of difference between different conditions and strains. ($p < 0.05$ was indicated and if or $> 0.05$ (ns).) For normal distribution the following formula was applied. The variable σ stands for standard deviation whereas μ stands for mean.

$$f(x) = \frac{1}{\sigma\sqrt{2\pi}} e^{-\frac{1}{2}\left(\frac{x-\mu}{\sigma}\right)^2}$$

# Chapter 3: RESULTS

## *3.1 EzColocalization Plugin to analyze Atg18 localization at the vacuole membrane*

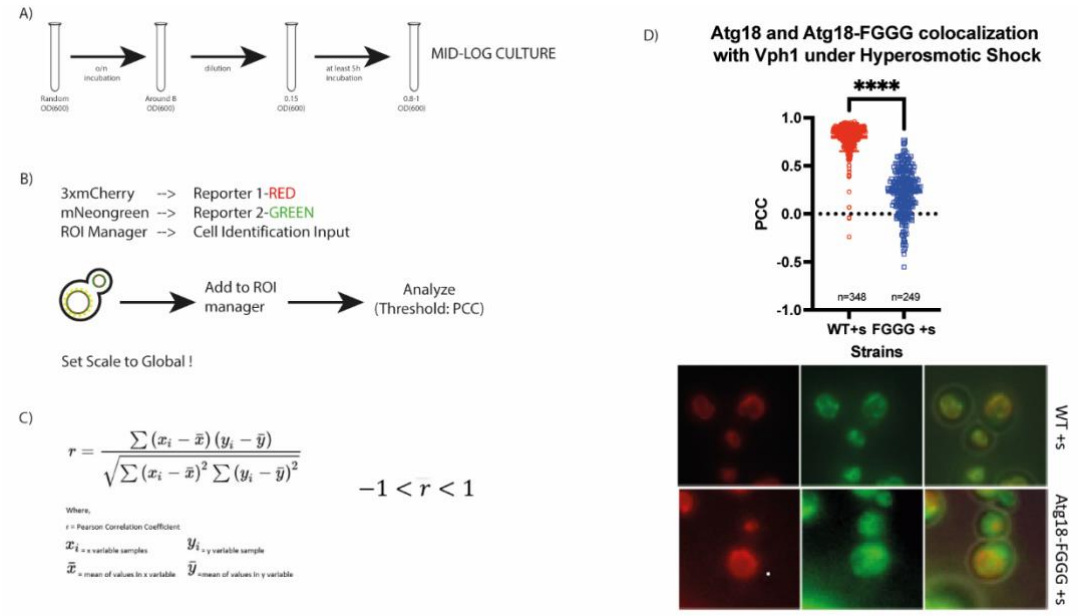


**Figure 3-1: What is Pearson Correlation Coefficient and How did I do my experiments?**

In this figure how I have done PCC measurements using EzColocalization plugin A) The incubation and dilution steps in order to have a mid-log yeast culture. B) The writings and the scheme represents how to work with EzColocalization plugin in ImageJ-FIJI. C) Mathematical calculation of PCC. x and y can be taken as reporter 1 and reporter 2 fluorescence intensity. D) The comparison of wild-type Atg18 and Atg18-FGGG mutant that cannot bind any phoshoinositides colocalization with Vph1-mCherry which is used as vacuole marker along with representative images

It was shown that Atg18 asymmetrically localizes to the daughter vacuoles at a certain time window during the cell cycle of baker's yeast (Dilege, 2022). Prior analysis was qualitative, and localization was decided through judgment by educated eyes. Quantification of localization was required for a better analysis. In this thesis, to cover this issue, I exploited Pearson's Correlation Coefficient (PCC) (figure 3-1 C) provided by a plugin named EzColocalization in ImageJ-FIJI (The link for the plugin is provided in the materials and methods section.). Vph1, V-ATPase channel, is found on the membrane of the yeast vacuole. Thus, I used Vph1 tagged with 3xmCherry at the C-terminus as a vacuole membrane marker. Our protein of interest,

Atg18, was tagged with mNeongreen (mNG). The plugin uses fluorescence intensity measured by the two signal and gives out a PCC value. The presence of the two signals similarly in one pixel gives out a number close to 1. Commenting on this PCC value, I can decide the co-localization of Atg18 with Vph1-3xmCherry on the vacuole numerically. Given that Vph1 is always present on the vacuole membrane, PCC value will tell us to what extend Atg18 localizes to the vacuole membrane. Therefore, the binary data for Atg18 localization at the vacuole periphery (localized or not localized) is replaced by a continuous value so that the changes in the amplitude of localization can be observed. While using the plugin, vacuoles were selected with the oval selection tool and the selections were saved with ROI manager (figure 3-1 B). Selecting the whole cell, instead of just selecting vacuoles, does not give a meaningful PCC value (Unpublished data of Mukadder Koyuncu) most likely due to presence of cytoplasmic signals which behaves randomly. For quantification of the colocalization, mid-log phase cell cultures were used in order to have cells that are in any stage during cell cycle (figure3-1A).
In previous research, it was concluded that PCC value between -0.5 and 0.5 does not provide any conclusion (Adler & Parmryd, 2010). Therefore, PCC scores less than 0.5 are treated as not colocalization, although these can be meaningful in some experiments (Parmryd et al., 2003). ATG18-FGGG, an Atg18 mutant that cannot bind neither PI(3,5)P2 nor PI3P (Gopaldass et al., 2017), thus, provides us a negative control since it won't be binding phosphoinositols on the surface of vacuoles. In the analysis of this mutant, PCC scores came much lower than 0.5. This allows us to trust the threshold provided by the former research (Adler & Parmryd, 2010).
The FGGG mutation does not show any colocalization. Although there is significant differences in PCC scores of different PI(3,5)$P_2$ elevating conditions, all these scores are much less than 0.5; therefore there is no colocalization (Figure 3-2 D).

## *3.2 ATG18 Localization to the Vacuole Increases in the Conditions where PI(3,5)P2 Levels are Elevated and PI(3,5)P2 Effectors Have an Impact on this Localization*

In this part, I investigated how Atg18 colocalization with Vph1 changes under conditions that interfere with PI(3,5)$P_2$ synthesis. PI(3,5)P2 levels are elevated upon hyperosmotic shock (0.9M NaCl) (Jin et al., 2016) In addition, a hyperactive mutant of *FAB1*, *fab1-14* (hereafter will be referred as *fab1-HyperActive*, *fab1-ha*), leads to over production of PI(3,5)P2 (Duex et al., 2006). Thus, I used hyperosmotic shock and the *fab1-ha* mutant, as conditions that causes increased PI(3,5)P2 production.

PCC values of Atg18-mNG colocalization with Vph1-3mCherry was ~0.6 under basal conditions (Figure 3-2 A). Under hyperosmotic shock and upon *fab1-ha* expression PCC values increased to ~0.8 and ~0.7 respectively (Figure 3-2 A). Hyperosmotic shock treatment of *fab1-ha* led to a PCC value of 0.8 (Figure 3-2 A). These changes in PCC values are in line with the reported changes in the levels of PI(3,5)P2 (Botelho et al., 2008; Duex et al., 2006) as well as the observed Atg18 localization at the vacuole periphery (Dilege, 2022; Obara et al., 2008) (Figure 3-2 A). Thus, our data supports that Atg18 vacuole periphery localization increases under conditions where PI(3,5)P2 levels are elevated.

The FGGG mutation does not show any colocalization. Although there are significant differences in PCC scores of different PI(3,5)P2 elevating conditions, all these scores are much less than 0.5; therefore there is no colocalization (Figure 3-2 B).

Aforementioned data indicate that the Atg18 vacuole periphery localization correlates with PI(3,5)P2 levels. Atg18 can bind both PI3P and PI3,5P2. To confirm that the observed vacuole localization is due to Atg18 binding to PI(3,5)P2 but not to the PI3P, I made use of the Atg18-Sloop mutant, which cannot bind PI3P, but can bind to PI(3,5)P2 albeit at a lesser extent than the wild type Atg18 (Gopaldass et al., 2017). Atg18-Sloop mutant gave a PCC score of ~ 0.4 under basal conditions (Figure 3-2 C, basal). When PI(3,5)P2 levels were increased, PCC scores also went up (Figure 3-2 C). Sole hyperosmotic shock raised the colocalization most, where either both or sole hyperactive mutant resulted similar PCC scores that are less than sole hyperosmotic shock and more than 0.5. (Figure 3-2 C). This suggests that the localization of Atg18-Sloop mutant increases as $PI(3,5)P_2$ levels increase as well.

I next analyzed Atg18-mNG localization at the vacuole membrane in cells lacking V*AC14* (*vac14*Δ) and *VAC7* (*vac7*Δ). Both Vac14 and Vac7 are important for PI(3,5)P2 synthesis (McCartney et al., 2014), thus PI(3,5)P2 levels diminish in *vac14*Δ and *vac7*Δ cells (Jin et al., 2008). Reflecting the diminished levels of PI3,5P2, PCC scores of Atg18 localization on the vacuoles were less than 0.5 in *vac14*Δ and *vac7*Δ cells under basal condition (Figure 3-2 D and E). Fab1-ha mutant promotes PI(3,5)P2 production also in the absence of Vac7 and Vac14. Similarly, introduction of *fab1-ha* in *vac14*Δ and *vac7*Δ cells caused elevation of PCC values above 0.5 (Figure 3-2 D and E). Hyperosmotic shock however affected *vac14*Δ and *vac7*Δ cells differently. Whereas salt treatment increased PCC values above 0.5 in *vac14*Δ cells, in *vac7*Δ cells it did not affect it (Figure 3-2 D and E). This result is also in line with the previous measurements of PI(3,5)P2 levels in *vac14*Δ and *vac7*Δ cells (Duex et al., 2006).

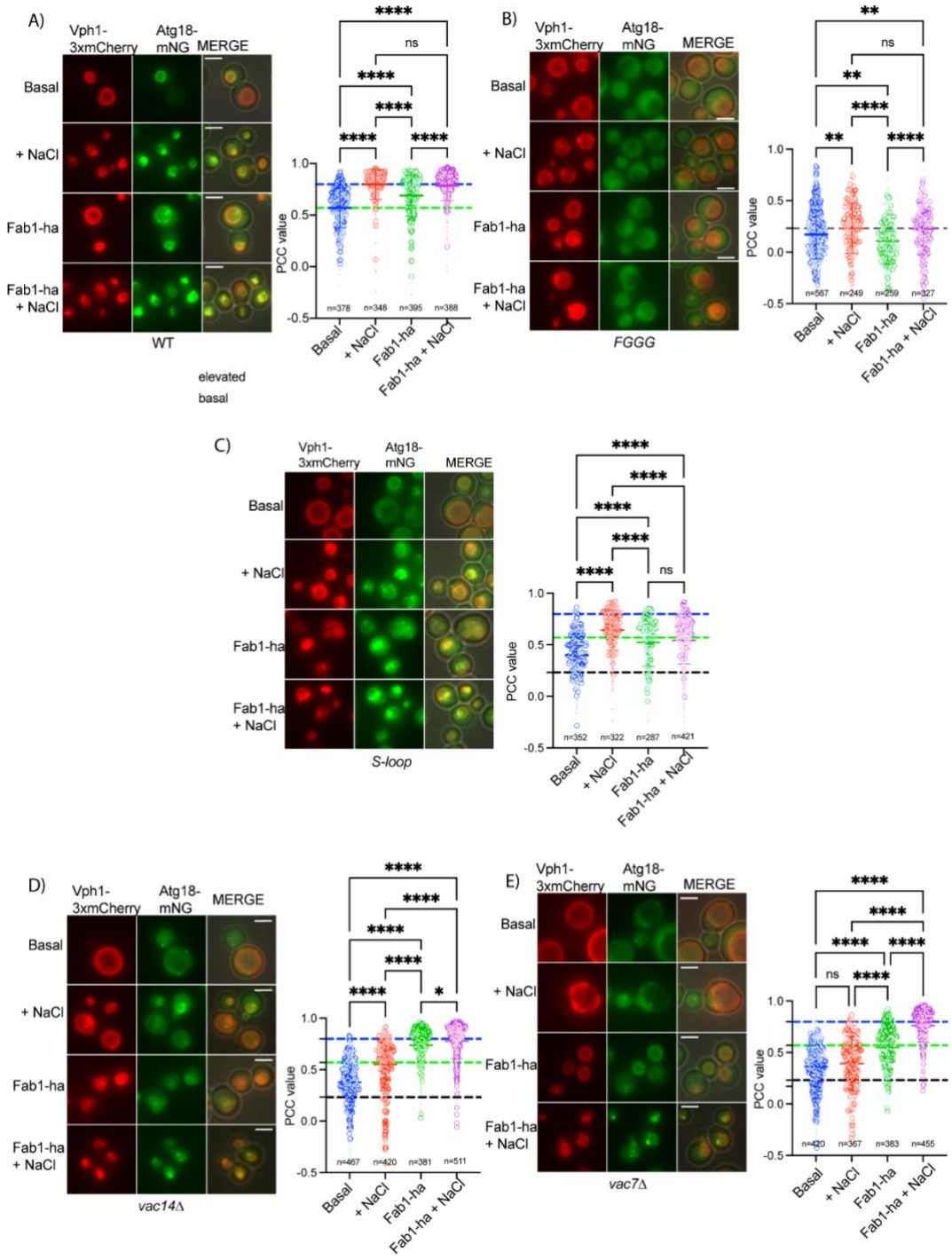


**Figure 3-2:The change of localization of ATG18-mNeongreen upon differently induced elevation of PI35P2 levels in different mutants.**

PCC value, Pearson coefficient, was provided by EzColocalization plugin in ImageJ-FIJI. It represents colocalization in the scale between -1 and 1. 1 means 100% colocalization, 0 means solely random which means two different channels neither attract nor push each other, and -1 means two different channels push each other. A) ATG18-mNeongreen and VPH1-mCherry colocalization in wild-type strain is shown. B) ATG18-FGGG-mNeongreen and VPH1-mCherry colocalization in wild-type strain is shown. C) ATG18-

Sloop-mNeongreen and VPH1-mCherry colocalization in wild-type strain is shown. D) ATG18-mNeongreen and VPH1-mCherry colocalization in vac14Δ strain is shown. E) ATG18-mNeongreen and VPH1-mCherry colocalization in vac7Δ strain is shown. There are two different sets of experiments in each graph. The graphs were plotted with Prism8.GraphPad. The number of cells counted was shown on the graphs. One-way ANOVA was performed to compare colocalization in different strains, where; *: $p<0.05$:, **:$p< 0.002$, ***: $p= 0.0001$ and ****: $p < 0.0001$.

## *3.3 ATG18 Asymmetrically Localizes to the Daughter Vacuole after Vacuole Segregation and Stays There for 30 Minutes in Average*

In our previous experiments, it was observed that Atg18 specifically localizes to daughter cell throughout the cell cycle (Dilege, 2022). However, the fluorophore attached to GFP and GFP bound to Atg18 was a giving relatively low signal, which may have prevented observation of Atg18 in half of the population of cells. To understand whether the lack of localization is due to low signal/noise, in this thesis, Atg18-mNeongreen was used in order to improve the signal. Vph1-3mcherry marked the vacuole membrane. In the timelapse, it was observed that two adjacent yeasts show daughter-specific localization (Figure 3-3 A).

Timelapse analysis using Atg18-mNG supported daughter vacuole specific Atg18 localization (Figure x any y selected time frames and PCC figure). Pearson Correlation Coefficient score was also measured for all cells that are budding throughout the timelapse. It was decided that the best way to represent PCC scores is drawing a point graph centering the vacuole segregation. Three points before and six points after vacuole segregation were taken into account for all counted cells. The average and error bars were represented. Daughter-specific localization can be differentiated easily as the signal on the mother vacuole drops beneath 0.5 (Figure 3-3 B).

In almost all cells analyzed Atg18 localized to daughter vacuole specifically at some point after vacuole segregation (Figure 3-3 C and D). Atg18 stayed on the daughter vacuole for an average of 30 minutes (Figure 3-3 E). Vast majority of the cells established daughter specific Atg18 localization at their vacuoles just after vacuole segregated to the daughter cell (Figure 3-3 F). All these data established that Atg18 exhibits an asymmetric localization preferably localizing on the daughter vacuole after vacuole segregation.

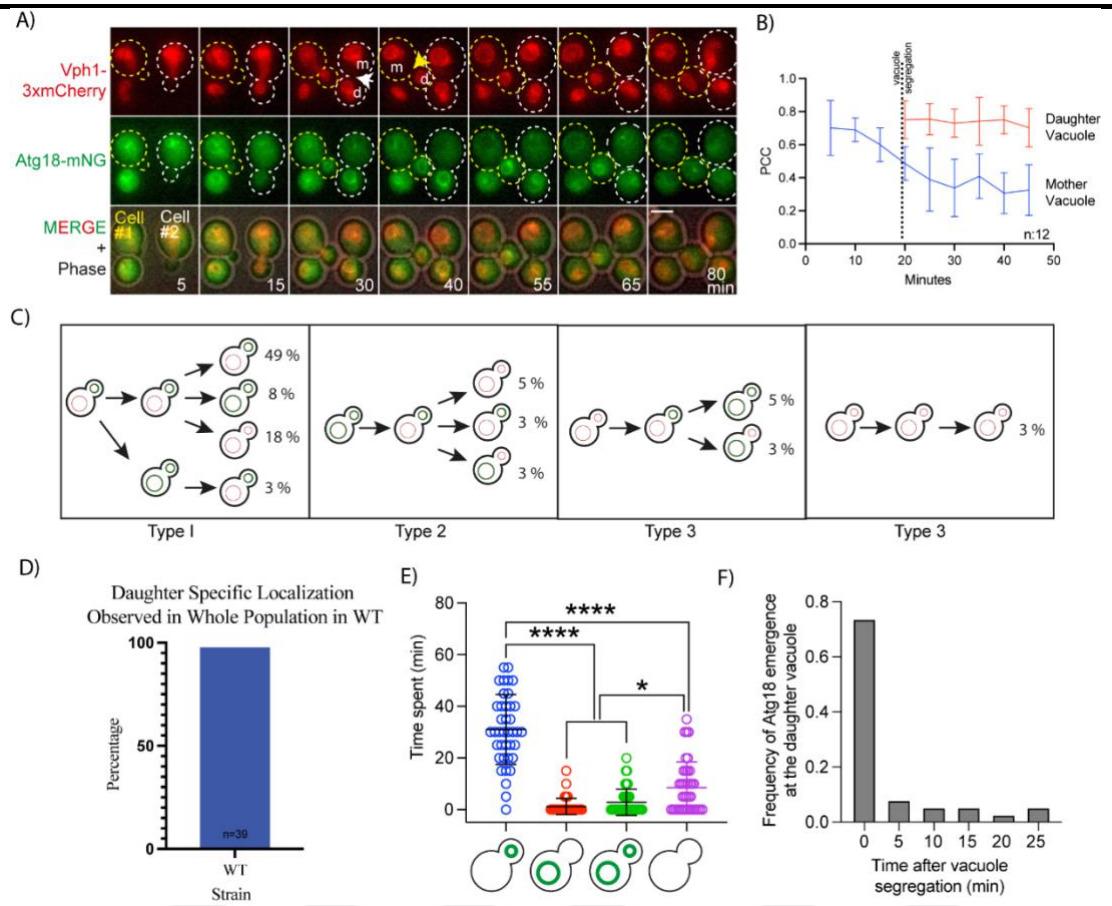


**Figure 3-3:The analysis of timelapse of ATG18-mNeongreen, VPH1-mCherry strain**

A) Representative images of the timelapse. The timelapse had 5-minute intervals, and mCherry and FITC filters were used. Max projection of z-stacks was taken. B) PCC values of mother and daughter vacuole were measured throughout the cell cycle. 3 points before and 6 points after the vacuole segregation were selected to observe PCC change. Before vacuole segregation, there was only the mother. The standard deviation and average of the data set were taken the graph was plotted in GraphPad. Cells starting from no or small bud were taken into account. C) How ATG18-mNeongreen behaved after vacuole segregation was plotted and the percentage of that behavior over the population number was denoted. D) How much percentage of the cells presented ATG18-mNeongreen localization to VPH1-mCherry tagged vacuoles were shown. E) How many minutes; and in which compartment, mother or daughter; the ATG18-mNeongreen signal was persisted were plotted. The first is daughter-specific, the second is mother-specific, the third is both, and the last one is no signal. One-way ANOVA was performed to compare different localizations, where; *: $p<0.05$:, **:$p< 0.002$, ***: $p= 0.0001$ and ****: $p < 0.0001$. F) Daughter-specific localization was seen after how many minutes from vacuole segregation was showed in percentage ratio.

## *3.4 Daughter Specific Localization Takes Place around the Time Anaphase Occurs*

The vacuolar vesicles pinched off from the mother vacuole travelling to daughter cell may be called segregation structure. Once this pinches of and placed in the daughter cell it is called

daughter vacuole. Here, Tub1 is tagged with mCherry fluorophore from its N-terminal helping us to decide in which cell-cycle phase is the budding yeast. Relatively thick and short spindle within the borders of mother cell is meant to be in metaphase transition. At the onset of anaphase, spindle elongates and then it reaches to the opposite poles of mother and daughter cell at late anaphase. Upon mimtotic exit, spindle breaks down and the cell continues to cytokinesis (Winey & O'Toole, 2001). Metaphase anaphase transition event occurs in less than 5 minutes. Considering this, the two points are always adjacent in timeline. Due to lack of tools, vacuole marker cannot be utilized in this experiment set up. Thus, it is assumed that Atg18 is on the vacuole when mNeongreen signal is circular, vesicle like (Figure 3-4 A). With this assumption I found that in the majority of cells Atg18 localizes solely to daughter vacuole within 5 minutes before and after from metaphase and persists until 5 minutes later than spindle breakdown (Figure 3-4 B and C).

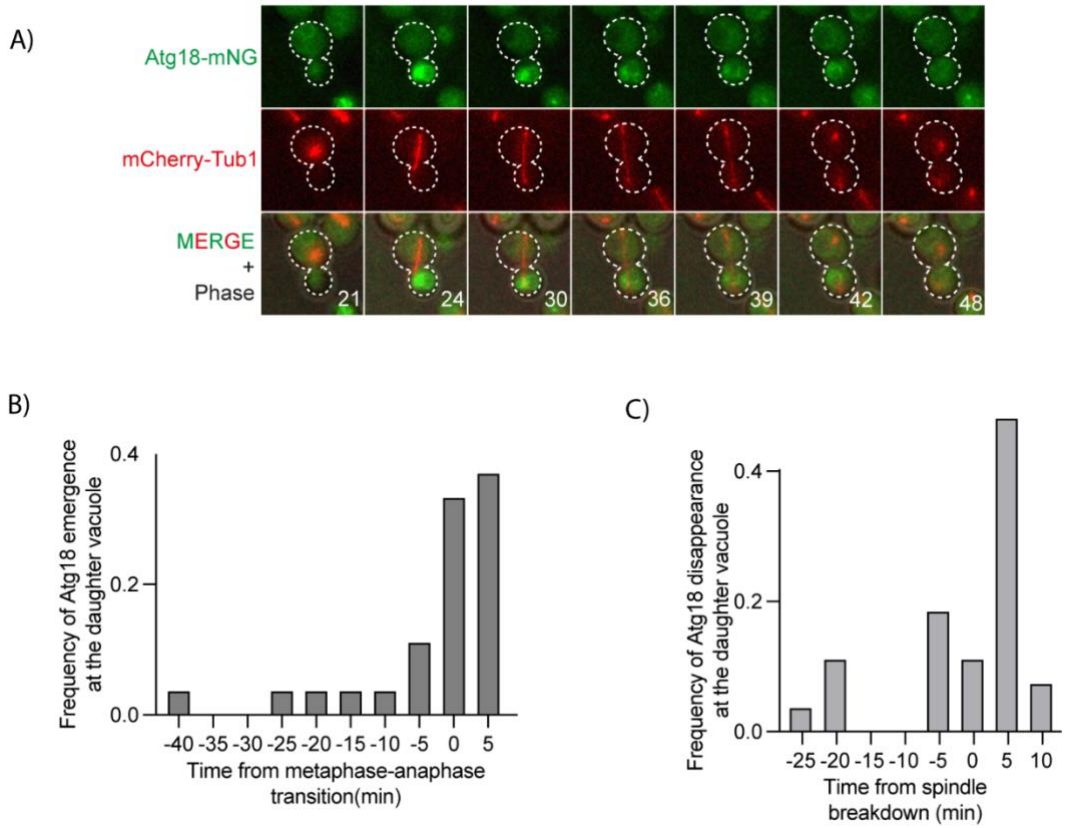


**Figure 3-4: The analysis of timelapse of the ATG18-mNeongreen and mCherry-TUB1 strain.**

A) This is the representative image of the timelapse. The interval of each time point is 3 minutes. FITC and mCherry filters were used. B) The histogram of the emergence of ATG18-mNeongreen signal on the daughter vacuole only related to metaphase anaphase transition in time. C) The histogram of the disappearance of ATG18-mNeongreen signal on the daughter vacuole only related to metaphase anaphase transition in time.

## *3.5 Do PI(3,5)P2 effector Vac14 also Asymmetrically Localizes to the Daughter Vacuole?*

In search of asymmetric localization of other $PI(3,5)P_2$ regulators, timelapse of Vac14 was done. In this timelapse, there is no daughter-specific localization of Atg18 was observed. Again, using PCC, colocalization was quantified and scores above 0.5 were observed for both mother and daughter vacuole after vacuole segregation.

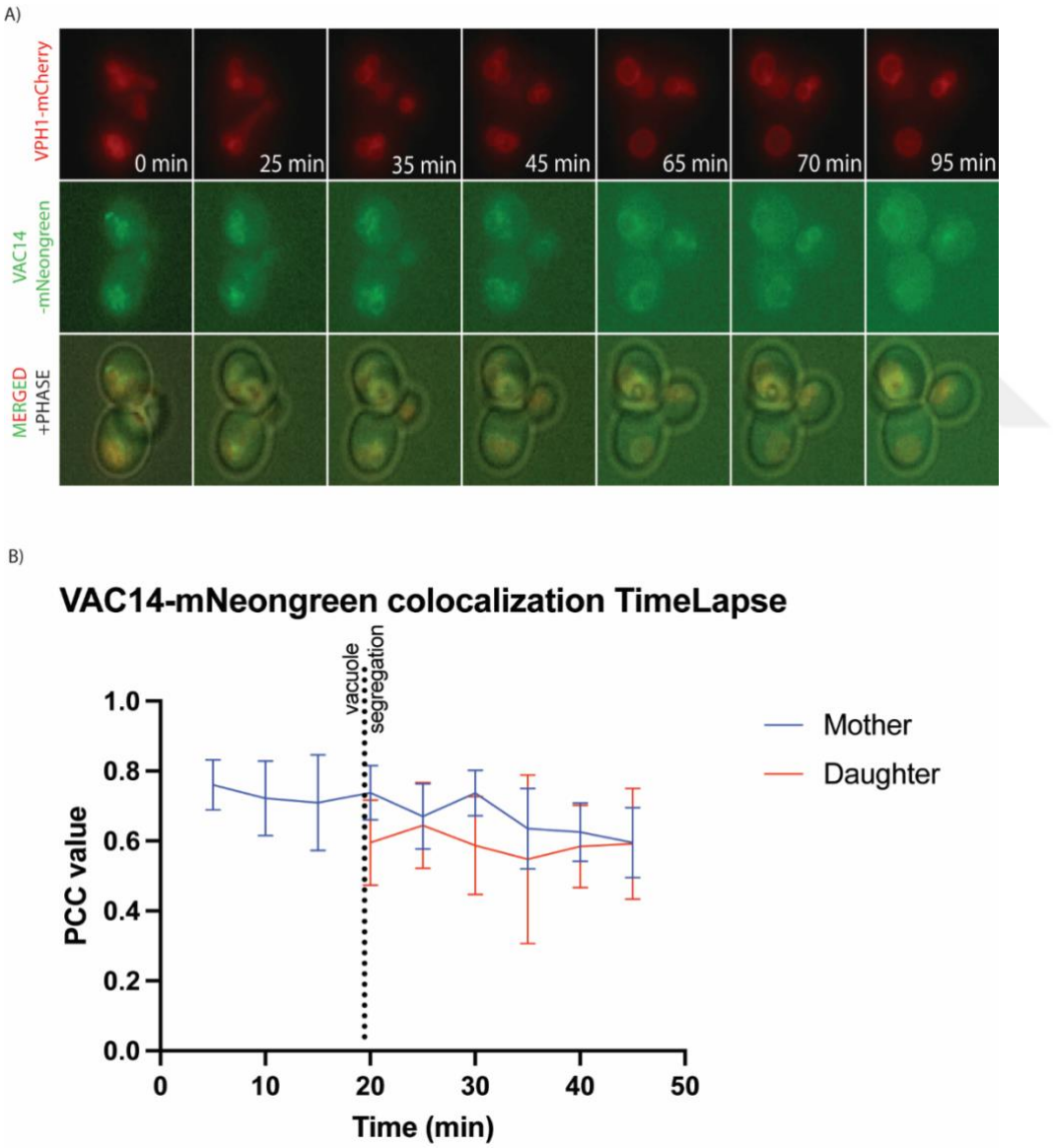


**Figure 3-5:The analysis of the timelapse of VAC14-mNeongreen and VPH1-mCherry**

Vac14 timelapse analysis. A)Representative images of the timelapse. The timelapse had 5-minute intervals, and mCherry and FITC filters were used. Max projection of z-stacks was taken. B) PCC values of mother and daughter vacuole were measured throughout the cell cycle. 3 points before and 6 points after the vacuole segregation were selected to observe PCC change. Before vacuole segregation, there was only the mother. The standard deviation and average of the data set were taken the graph was plotted in GraphPad. Cells starting from no or small bud were considered.

## *3.6 Can Asymmetry be Shown other than the Timelapse Method?*

Using timelapse for many strains was time consuming initially. Plus, not all proteins were able to be observed via timelapse since either they give very low signals or photobleach quickly. Therefore, another way to observe daughter-specific localization was sought for quicker analysis. Instead I quantified the daughter vacuole to mother vacuole ratio of the fluorescence intensity of the protein of interest (see material methods *2.3.2.1 Fluorescence-based Manual Analysis* for details). Here, only cells with segregated vacuoles were counted. To better visualize whether more protein is present on the daughter vacuole then on the mother vacuole, the natural logarithm of the calculated ratios was plotted. As ln (1) equals zero, values greater than zero indicates daughter vacuole preference of the protein of interest. Likewise, values smaller than zero indicates mother vacuole preference, whereas values close to zero indicate equal localization at both vacuoles. Two ways were exploited to show how the population behaves: histogram, and probability distribution function (PDF). In histogram the distribution of ln of ratios were plotted. The normal distribution of these natural logarithm values provides us peaks which I can compare its position against x=0 line. When PDF values are plotted, if the peak is on the positive side it means that this protein has daughter-brighter signal whereas if the peak is on the negative side it means mother-brighter sign. This representation provides a good qualification of if the tagged proteins with green fluorophore have mother or daughter-brighter signal due to the location of the peak compared to x=0 line. Given this info, Atg18-mNeongreen, and Ivy1-mNeongreen are strongly daughter-brighter whereas Atg18-Sloop-mNeongreen is slightly daughter-brighter (Figure 3-6 – A, B, and H). Vac7, Vac14, and Fab1 showed equal brightness of mother and daughter vacuole (Figure 3-6 D, E, and F). Sch9, on the other hand, seems like its is slightly brighter on mother vacuole than the daughter vacuole (Figure 3-6, G). Atg18-FGGG-mNeongreen was analyzed as a negative control. This analysis provide us that when there is not localization at all, PDF amplitude is very low, there is no preference between mother and daughter and the values are scattered to the higher ratios (Figure 3-6 C). In order to be able to compare the results among each other two different graphs

were plotted. In figure 3-6 I, the comparison of probability distribution function of different proteins was given. In figure 3-6 J, box and violin plot was plotted. In both approaches, similar results can be seen as indicated before.

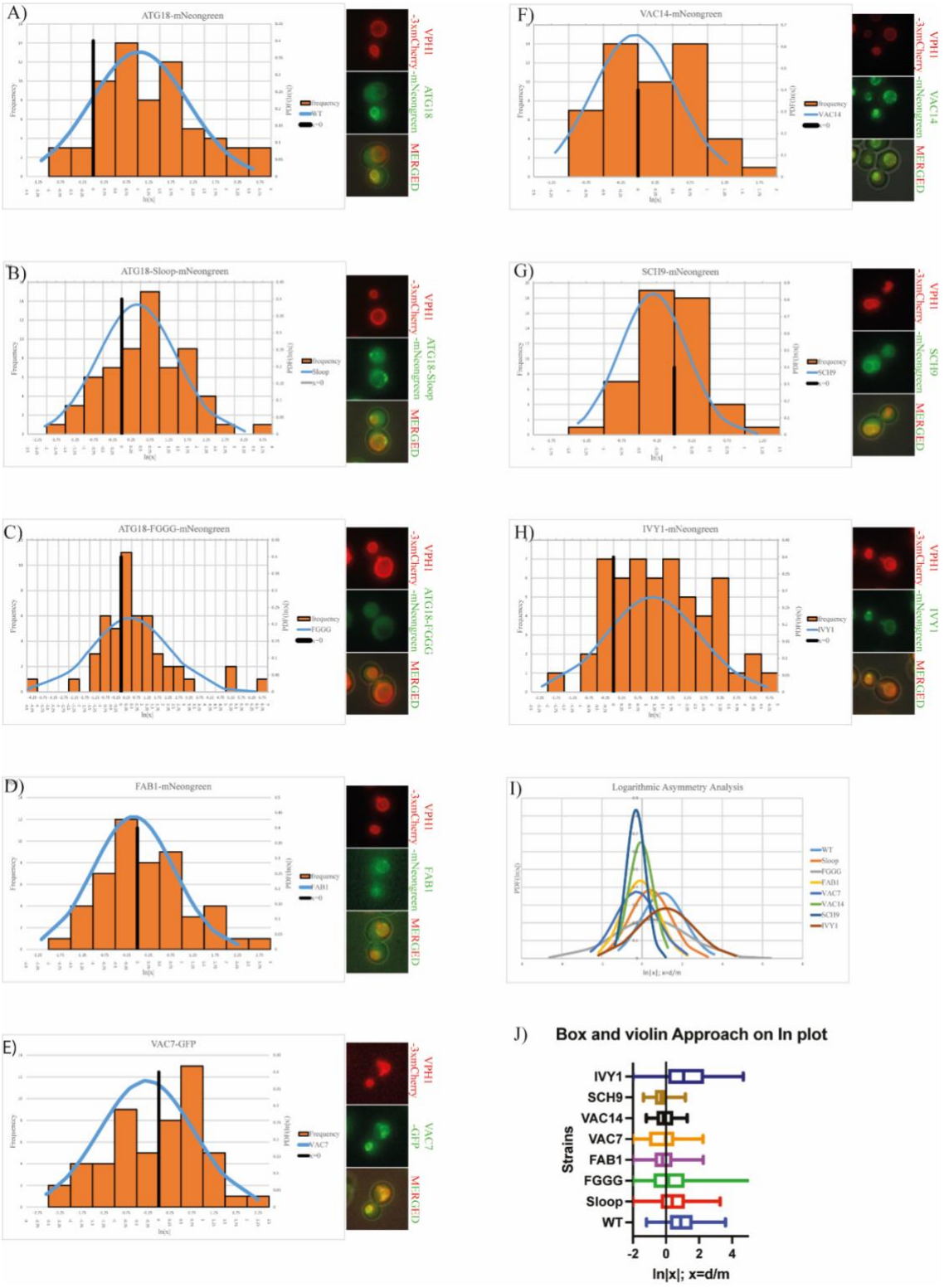

**Figure 3-6:Fluorescence intensity measurements to determine whether mother or daughter has a brighter mNeongreen or GFP signal.**

Orange bar graphs represent a histogram where the frequency values are on the left y-axis. The blue line represents the probability distribution function (PDF), where its outputs are represented on the right y-axis. The values of PDF are calculated with Excel's normal distribution function. The thick black line represents the x=0 line. PDF values are calculated by taking the natural logarithm of the absolute value of fluorescence intensity ratios. The ratios were calculated as explained in the materials and methods chapter. Therefore, the negative values represent mother-brighter cells, whereas positive values represent daughter-brighter.

# Chapter 4:DISCUSSION

In this study, I aimed to show Atg18 localization on vacuoles quantitatively in mutations of $PI(3,5)P_2$ regulators and elevated $PI(3,5)P_2$ levels along with Atg18 daughter-specific localization during cell cycle.

Atg18 binds to $PI(3,5)P_2$ on vacuoles of yeast cells and regulate the biosynthesis of $PI(3,5)P_2$ (Efe et al., 2007). In search of ways to quantify the localization of Atg18 to vacuoles, EzColocalization plugin for imageJ-FIJI was found to be the most eligible tool. This tool measures PCC, which is value for correlation that also can be investigated as colocalization. When $PI(3,5)P_2$ concentration was raised, by applying hyperosmotic shock, 0.9M NaCl media, yeast strains where one is wild-type Atg18 and the other is a variant of Atg18 (FGGG) that cannot bind any phosphoinositols, wild type Atg18 presented a PCC score around 0.7 while Atg18-FGGG presented much lower than 0.5 (PCC score of 0.5 was determined to be a threshold for colocalization.) This result showed us that this plugin can give meaningful quantization of localization of Atg18 to vacuoles. Further studies that require to measure localization, EzColocalization plugin can easily be utilized in the presence of proper fluorophores.

In the light of PCC scores, Atg18 slightly localizes to vacuoles with a score of around 0.6. This localization is strongly amplified upon increasing the $PI(3,5)P_2$ levels with two conditions: exposing the yeasts to hyperosmotic shock, or expressing the hyperactive Fab1 that phosphorylates PI3P to $PI(3,5)P_2$. PCC score of 0.8 can be evaluated as a strong localization in accordance with our results. When $PI(3,5)P_2$ levels are increased by these two conditions, the score of Atg18-FGGG remained much lower than 0.5 indicating that Atg18-FGGG does not localize on vacuoles. The score of this mutant served as a negative control for our experiments. Atg18-Sloop mutant which only binds $PI(3,5)P_2$ showed little or no localization to vacuoles while induced $PI(3,5)P_2$ levels made Atg18-Sloop localize to vacuoles with similar scores to wild type Atg18 in basal conditions. This finding can be due to either low levels of $PI(3,5)P_2$ (Balla, 2013), or its localization on microdomains on the periphery of the vacuoles (Takatori & Fujimoto, 2016). If Atg18-Sloop is not found around the vacuole but in microdomains, I would also expect a more heterogeneous mNeongreen signal. The patchy appearance reported before (Dilege, 2022) in Sloop mutants also may be due to the appearance of $PI(3,5)P_2$ in microdomains.

In the absence of Vac14, hyperosmotic shock appears to be able to increase $PI(3,5)P_2$ levels since Atg18 localization increases. However, in the absence of Vac7, $PI(3,5)P_2$ levels cannot rise with sole hyperosmotic shock. Knowing that Vac7 and Vac14 is required for Fab1 activity (Dove et al., 1997), in Vac14 defective cells $PI(3,5)P_2$ levels went up. It was previously shown that Vac14 and Fig4 is required for $PI(3,5)P_2$ turnover (Duex et al., 2006). The absence of Vac14 decreases the turnover rate of $PI(3,5)P_2$ and renders $PI(3,5)P_2$ stable still after 10 minutes of hyperosmotic stress working with Fig4 (Duex, Tang, et al., 2006). This may be why I see such difference in *VAC7* and *VAC14* deleted strains. On the other hand, Fab1-ha rescues localization of Atg18 to vacuoles in both deletions.

During investigation of Atg18 localization, daughter-specific localization of Atg18 during cell cycle came into notice (Dilege, 2022). Timelapse analyses of Atg18 localization was done to show this phenomenon. In these analyses 49% percent of the cells showed solely daughter-specific localization after vacuole segregation until cytokinesis, whereas almost all of the cells showed daughter specific localization at some point after vacuole segregation. In average cells Atg18 remained in the daughter vacuole for 30 minutes and this localization emerged within 5 minutes after vacuole segregation. Asymmetric localization of proteins during cell cycle is important to differentiate metabolism in old mother cell and newly emerging bud. The polarity is provided by cytoskeleton and motor proteins such as Myo2 and Myo4 (Fehrenbacher et al., 2004). The mediator proteins that bind to vesicles or proteins and their turnover rates regulate polarity, thus asymmetric localization, of proteins during cell cycle (Swayne et al., 2011; Tang et al., 2006). As an example, for such asymmetry, HO mating type switching gene can be given. Normally HO expression in mother may alter mating type; however, the daughter cells cannot. It was previously thought that the HO gene is silenced in the daughter cell. Eventually the reason why HO does not function in the daughter was found to be daughter specific localization of Ash1. Ash1 was suppressing the translation of HO gene (Amon, 1996). Atg18 being a member of PAS complex, it may take role in autophagy events that take place at the daughter-vacuole for specific proteins or vesicles.

Vacuole inheritance initiates before nuclear segregation (Weisman, 2003). In this study, timely correlation of daughter-specific Atg18 localization to the mitosis was investigated. It was found that daughter-specific Atg18 localization emerges mostly at the time, or 5 minutes later than metaphase-anaphase transition. Likewise, daughter-specific Atg18 localization mostly disappears 5 minutes after spindle breakdown. Here I can say that Atg18 localizes to daughter vacuole asymmetrically starts around metaphase and ends shotly after mitotic exit.

Next, I questioned whether other PI(3,5)$P_2$ regulators asymmetrically localize. I showed that Vac14 does not have neither mother nor daughter specificity during cell cycle with timelapse. Then I investigated mid-log phase culture of either GFP or mNeongreen tagged regulators and measured the fluorescence intensity of fluorescence on the vacuoles, then I plotted the natural logarithm of the ratio of green signal over red signal with histograms and PDFs. These plots showed that wild-type Atg18 showed brighter daughter vacuoles whereas Atg18-Sloop has slightly less brightness in green. Fab1, Vac7, and Vac14 did not show any skewness towards any site meaning that there is not neither mother nor daughter specific localization. Then I checked two interaction parts of Atg18: Sch9 and Ivy1. Sch9 has a central role in nutrient-sensing pathway by interacting with TORC1. For Sch9 to interact with TORC1, it is supposed to localize on the vacuole membrane. This localization depends on PI(3,5)$P_2$ although Sch9 does not have a conventional lipid binding domain (Deprez et al., 2023). On the other hand, Ivy1 is known to be the inhibitor of Fab1 (Malia et al., 2018). The histogram and PDF of Sch9 showed that it has brighter mother signal, therefore there might be mother-specific localization. The plots of Ivy1 showed a strong daughter-specific brightness suggesting that Ivy1 may localize to daughter asymmetrically. To denote, Ivy1 has very strong patchy localization observed in mother and daughter vacuole even though there is peripheral signal as well. This patchy signal might be daughter enriched. To unravel that mystery, further analyses are required.

This thesis, utilizing a quantization of localization method that can be used for timelapses, provides an eligible tool to analyze PI(3,5)$P_2$ regulators or its secondary regulators if they are asymmetric. This way, novel connections may be done among different pathways in terms of asymmetry.

To address the issue that if Atg18 can be utilized as PI(3,5)$P_2$ marker, this thesis suggests that Atg18 vacuole localization correlates with the PI(3,5)$P_2$ levels, thus it can be utilized as a PI(3,5)$P_2$ marker.

# BIBLIOGRAPHY

Adler, J., & Parmryd, I. (2010). Quantifying colocalization by correlation: The Pearson correlation coefficient is superior to the Mander's overlap coefficient. *Cytometry Part A*, *77A*(8), 733-742. https://doi.org/https://doi.org/10.1002/cyto.a.20896

Alberts, B., Johnson, A., Lewis, J., Raff, M., Roberts, K., & Walter, P. (2002). *Molecular biology of the cell* (4th ed.). Garland Science. http://bvbr.bib-bvb.de:8991/F?func=service&doc_library=BVB01&doc_number=009653135&line_number=0001&func_code=DB_RECORDS&service_type=MEDIA

Amon, A. (1996). Mother and daughter are doing fine: asymmetric cell division in yeast. *Cell*, *84*(5), 651-654.

Balla, T. (2013). Phosphoinositides: tiny lipids with giant impact on cell regulation. *Physiol Rev*, *93*(3), 1019-1137. https://doi.org/10.1152/physrev.00028.2012

Banerjee, S., Clapp, K., Tarsio, M., & Kane, P. M. (2019). Interaction of the late endo-lysosomal lipid PI(3,5)P2 with the Vph1 isoform of yeast V-ATPase increases its activity and cellular stress tolerance. *Journal of Biological Chemistry*, *294*(23), 9161-9171. https://doi.org/10.1074/jbc.RA119.008552

Banerjee, S., & Kane, P. M. (2020). Regulation of V-ATPase activity and organelle pH by phosphatidylinositol phosphate lipids. *Frontiers in Cell and Developmental Biology*, *8*, 510.

Barnum, K. J., & O'Connell, M. J. (2014). Cell Cycle Regulation by Checkpoints. In E. Noguchi & M. C. Gadaleta (Eds.), *Cell Cycle Control: Mechanisms and Protocols* (pp. 29-40). Springer New York. https://doi.org/10.1007/978-1-4939-0888-2_2

Bonangelino , C. J., Nau , J. J., Duex , J. E., Brinkman , M., Wurmser , A. E., Gary , J. D., Emr , S. D., & Weisman , L. S. (2002). Osmotic stress–induced increase of phosphatidylinositol 3,5-bisphosphate requires Vac14p, an activator of the lipid kinase Fab1p. *Journal of Cell Biology*, *156*(6), 1015-1028. https://doi.org/10.1083/jcb.200201002

Botelho, R. J., Efe, J. A., Teis, D., & Emr, S. D. (2008). Assembly of a Fab1 phosphoinositide kinase signaling complex requires the Fig4 phosphoinositide phosphatase. *Mol Biol Cell*, *19*(10), 4273-4286. https://doi.org/10.1091/mbc.e08-04-0405

Botstein, D., Chervitz, S. A., & Cherry, J. M. (1997). Yeast as a model organism. *Science*, *277*(5330), 1259-1260. https://doi.org/10.1126/science.277.5330.1259

Byers, B., & Goetsch, L. (1974). Duplication of spindle plaques and integration of the yeast cell cycle. Cold Spring Harbor symposia on quantitative biology,

Deprez, M.-A., Caligaris, M., Rosseels, J., Hatakeyama, R., Ghillebert, R., Sampaio-Marques, B., Mudholkar, K., Eskes, E., Meert, E., Ungermann, C., Ludovico, P., Rospert, S., De Virgilio, C., & Winderickx, J. (2023). The nutrient-responsive CDK Pho85 primes the Sch9 kinase for its activation by TORC1. *PLOS Genetics*, *19*(2), e1010641. https://doi.org/10.1371/journal.pgen.1010641

Desfougères, Y., Vavassori, S., Rompf, M., Gerasimaite, R., & Mayer, A. (2016). Organelle acidification negatively regulates vacuole membrane fusion in vivo. *Scientific Reports*, *6*(1), 29045. https://doi.org/10.1038/srep29045

Dilege, C. (2022). *ANALYSIS OF PI(3,5)P2 THROUGHOUT MITOSIS* [Dissertation, Koc University].

Dong, X.-p., Shen, D., Wang, X., Dawson, T., Li, X., Zhang, Q., Cheng, X., Zhang, Y., Weisman, L. S., Delling, M., & Xu, H. (2010). PI(3,5)P2 controls membrane trafficking by direct activation of mucolipin Ca2+ release channels in the

endolysosome. *Nature Communications*, *1*(1), 38. https://doi.org/10.1038/ncomms1037

Dove, S. K., Cooke, F. T., Douglas, M. R., Sayers, L. G., Parker, P. J., & Michell, R. H. (1997). Osmotic stress activates phosphatidylinositol-3,5-bisphosphate synthesis. *Nature*, *390*(6656), 187-192. https://doi.org/10.1038/36613

Duex, J. E., Nau, J. J., Kauffman, E. J., & Weisman, L. S. (2006). Phosphoinositide 5-phosphatase Fig 4p is required for both acute rise and subsequent fall in stress-induced phosphatidylinositol 3,5-bisphosphate levels. *Eukaryot Cell*, *5*(4), 723-731. https://doi.org/10.1128/ec.5.4.723-731.2006

Duex, J. E., Tang, F., & Weisman, L. S. (2006). The Vac14p-Fig4p complex acts independently of Vac7p and couples PI3,5P2 synthesis and turnover. *J Cell Biol*, *172*(5), 693-704. https://doi.org/10.1083/jcb.200512105

Efe, J., Botelho, R., & Emr, S. (2007). Atg18 Regulates Organelle Morphology and Fab1 Kinase Activity Independent of Its Membrane Recruitment by Phosphatidylinositol 3,5-Bisphosphate. *Molecular Biology of the Cell*, *18*, 4232-4244. https://doi.org/10.1091/mbc.E07-04-0301

Fehrenbacher, K. L., Yang, H.-C., Gay, A. C., Huckaba, T. M., & Pon, L. A. (2004). Live cell imaging of mitochondrial movement along actin cables in budding yeast. *Current Biology*, *14*(22), 1996-2004.

Gary, J. D., Sato, T. K., Stefan, C. J., Bonangelino, C. J., Weisman, L. S., & Emr, S. D. (2002). Regulation of Fab1 phosphatidylinositol 3-phosphate 5-kinase pathway by Vac7 protein and Fig4, a polyphosphoinositide phosphatase family member. *Mol Biol Cell*, *13*(4), 1238-1251. https://doi.org/10.1091/mbc.01-10-0498

Gary, J. D., Wurmser, A. E., Bonangelino, C. J., Weisman, L. S., & Emr, S. D. (1998). Fab1p is essential for PtdIns (3) P 5-kinase activity and the maintenance of vacuolar size and membrane homeostasis. *The Journal of cell biology*, *143*(1), 65-79.

Gopaldass, N., Fauvet, B., Lashuel, H., Roux, A., & Mayer, A. (2017). Membrane scission driven by the PROPPIN Atg18. *Embo j*, *36*(22), 3274-3291. https://doi.org/10.15252/embj.201796859

Harding, T. M., Hefner-Gravink, A., Thumm, M., & Klionsky, D. J. (1996). Genetic and phenotypic overlap between autophagy and the cytoplasm to vacuole protein targeting pathway. *Journal of Biological Chemistry*, *271*(30), 17621-17624.

Hartwell, L. H., & Unger, M. W. (1977). Unequal division in Saccharomyces cerevisiae and its implications for the control of cell division. *J Cell Biol*, *75*(2 Pt 1), 422-435. https://doi.org/10.1083/jcb.75.2.422

Hasegawa, J., Strunk, B. S., & Weisman, L. S. (2017). PI5P and PI(3,5)P(2): Minor, but Essential Phosphoinositides. *Cell Struct Funct*, *42*(1), 49-60. https://doi.org/10.1247/csf.17003

Ho, C. Y., Alghamdi, T. A., & Botelho, R. J. (2012). Phosphatidylinositol-3,5-Bisphosphate: No Longer the Poor PIP2. *Traffic*, *13*(1), 1-8. https://doi.org/https://doi.org/10.1111/j.1600-0854.2011.01246.x

Horazdovsky, B. F., Busch, G. R., & Emr, S. D. (1994). VPS21 encodes a rab5-like GTP binding protein that is required for the sorting of yeast vacuolar proteins. *Embo j*, *13*(6), 1297-1309. https://doi.org/10.1002/j.1460-2075.1994.tb06382.x

Ishikawa, K., Catlett, N. L., Novak, J. L., Tang, F., Nau, J. J., & Weisman, L. S. (2003). Identification of an organelle-specific myosin V receptor. *J Cell Biol*, *160*(6), 887-897. https://doi.org/10.1083/jcb.200210139

Jin, N., Chow, C. Y., Liu, L., Zolov, S. N., Bronson, R., Davisson, M., Petersen, J. L., Zhang, Y., Park, S., Duex, J. E., Goldowitz, D., Meisler, M. H., & Weisman, L. S. (2008).

VAC14 nucleates a protein complex essential for the acute interconversion of PI3P and PI(3,5)P2 in yeast and mouse. *The EMBO Journal*, *27*(24), 3221-3234. https://doi.org/https://doi.org/10.1038/emboj.2008.248

Jin, N., Lang, M. J., & Weisman, L. S. (2016). Phosphatidylinositol 3,5-bisphosphate: regulation of cellular events in space and time. *Biochem Soc Trans*, *44*(1), 177-184. https://doi.org/10.1042/bst20150174

Klionsky, D. J., Cregg, J. M., Dunn, W. A., Emr, S. D., Sakai, Y., Sandoval, I. V., Sibirny, A., Subramani, S., Thumm, M., & Veenhuis, M. (2003). A unified nomenclature for yeast autophagy-related genes. *Developmental cell*, *5*(4), 539-545.

Kotani, T., Kirisako, H., Koizumi, M., Ohsumi, Y., & Nakatogawa, H. (2018). The Atg2-Atg18 complex tethers pre-autophagosomal membranes to the endoplasmic reticulum for autophagosome formation. *Proceedings of the National Academy of Sciences*, *115*(41), 10363-10368. https://doi.org/doi:10.1073/pnas.1806727115

Levine, T. P. (2022). TMEM106B in humans and Vac7 and Tag1 in yeast are predicted to be lipid transfer proteins. *Proteins: Structure, Function, and Bioinformatics*, *90*(1), 164-175. https://doi.org/https://doi.org/10.1002/prot.26201

Li, S. C., Diakov, T. T., Xu, T., Tarsio, M., Zhu, W., Couoh-Cardel, S., Weisman, L. S., & Kane, P. M. (2014). The signaling lipid PI(3,5)P2 stabilizes V1–Vo sector interactions and activates the V-ATPase. *Molecular Biology of the Cell*, *25*(8), 1251-1262. https://doi.org/10.1091/mbc.e13-10-0563

Malia, P., Numrich, J., Nishimura, T., González Montoro, A., Stefan, C. J., & Ungermann, C. (2018). Control of vacuole membrane homeostasis by a resident PI-3,5-kinase inhibitor. *Proceedings of the National Academy of Sciences*, *115*(18), 4684-4689. https://doi.org/doi:10.1073/pnas.1722517115

McCartney, A. J., Zhang, Y., & Weisman, L. S. (2014). Phosphatidylinositol 3, 5-bisphosphate: low abundance, high significance. *BioEssays*, *36*(1), 52-64.

Morgan, D. O., & New Science, P. (2007). *The cell cycle : principles of control*. New Science Press ;

Sinauer Associates. http://www.new-science-press.com/browse/cellcycle/contents/

Suzuki, K., & Ohsumi, Y. (2010). Current knowledge of the pre-autophagosomal structure (PAS). *FEBS Letters*, *584*(7), 1280-1286. https://doi.org/https://doi.org/10.1016/j.febslet.2010.02.001

Nielsen, J. (2019). Yeast Systems Biology: Model Organism and Cell Factory. *Biotechnology Journal*, *14*(9), 1800421. https://doi.org/https://doi.org/10.1002/biot.201800421

Obara, K., Sekito, T., Niimi, K., & Ohsumi, Y. (2008). The Atg18-Atg2 complex is recruited to autophagic membranes via phosphatidylinositol 3-phosphate and exerts an essential function. *J Biol Chem*, *283*(35), 23972-23980. https://doi.org/10.1074/jbc.M803180200

Palamiuc, L., Ravi, A., & Emerling, B. M. (2020). Phosphoinositides in autophagy: current roles and future insights. *The FEBS Journal*, *287*(2), 222-238. https://doi.org/https://doi.org/10.1111/febs.15127

Pan, X., Roberts, P., Chen, Y., Kvam, E., Shulga, N., Huang, K., Lemmon, S., & Goldfarb, D. S. (2000). Nucleus-vacuole junctions in Saccharomyces cerevisiae are formed through the direct interaction of Vac8p with Nvj1p. *Mol Biol Cell*, *11*(7), 2445-2457. https://doi.org/10.1091/mbc.11.7.2445

Parmryd, I., Adler, J., Patel, R., & Magee, A. I. (2003). Imaging metabolism of phosphatidylinositol 4,5-bisphosphate in T-cell GM1-enriched domains containing Ras proteins. *Exp Cell Res*, *285*(1), 27-38. https://doi.org/10.1016/s0014-4827(02)00048-4

Posor, Y., Jang, W., & Haucke, V. (2022). Phosphoinositides as membrane organizers. *Nature Reviews Molecular Cell Biology*, *23*(12), 797-816. https://doi.org/10.1038/s41580-022-00490-x

Raymond, C. K., O'Hara, P. J., Eichinger, G., Rothman, J. H., & Stevens, T. H. (1990). Molecular analysis of the yeast VPS3 gene and the role of its product in vacuolar protein sorting and vacuolar segregation during the cell cycle. *The Journal of cell biology*, *111*(3), 877-892.

Rudge, S. A., Anderson, D. M., & Emr, S. D. (2004). Vacuole size control: regulation of PtdIns(3,5)P2 levels by the vacuole-associated Vac14-Fig4 complex, a PtdIns(3,5)P2-specific phosphatase. *Mol Biol Cell*, *15*(1), 24-36. https://doi.org/10.1091/mbc.e03-05-0297

Sbrissa, D., Ikonomov, O. C., & Shisheva, A. (2002). Phosphatidylinositol 3-phosphate-interacting domains in PIKfyve. Binding specificity and role in PIKfyve. Endomenbrane localization. *J Biol Chem*, *277*(8), 6073-6079. https://doi.org/10.1074/jbc.M110194200

Schulze, U., Vollenbröker, B., Braun, D. A., Van Le, T., Granado, D., Kremerskothen, J., Fränzel, B., Klosowski, R., Barth, J., & Fufezan, C. (2014). The Vac14-interaction network is linked to regulators of the endolysosomal and autophagic pathway. *Molecular & Cellular Proteomics*, *13*(6), 1397-1411.

Scott, S. V., Nice, D. C., 3rd, Nau, J. J., Weisman, L. S., Kamada, Y., Keizer-Gunnink, I., Funakoshi, T., Veenhuis, M., Ohsumi, Y., & Klionsky, D. J. (2000). Apg13p and Vac8p are part of a complex of phosphoproteins that are required for cytoplasm to vacuole targeting. *J Biol Chem*, *275*(33), 25840-25849. https://doi.org/10.1074/jbc.M002813200

Singer-Krüger, B., Stenmark, H., & Zerial, M. (1995). Yeast Ypt51p and mammalian Rab5: counterparts with similar function in the early endocytic pathway. *J Cell Sci*, *108 ( Pt 11)*, 3509-3521. https://doi.org/10.1242/jcs.108.11.3509

Strunk, B. S., Steinfeld, N., Lee, S., Jin, N., Muñoz-Rivera, C., Meeks, G., Thomas, A., Akemann, C., Mapp, A. K., MacGurn, J. A., & Weisman, L. S. (2020). Roles for a lipid phosphatase in the activation of its opposing lipid kinase. *Molecular Biology of the Cell*, *31*(17), 1835-1845. https://doi.org/10.1091/mbc.E18-09-0556

Suzuki, K., & Ohsumi, Y. (2010). Current knowledge of the pre-autophagosomal structure (PAS). *FEBS Letters*, *584*(7), 1280-1286. https://doi.org/https://doi.org/10.1016/j.febslet.2010.02.001

Swayne, T. C., Zhou, C., Boldogh, I. R., Charalel, J. K., McFaline-Figueroa, J. R., Thoms, S., Yang, C., Leung, G., McInnes, J., & Erdmann, R. (2011). Role for cER and Mmr1p in anchorage of mitochondria at sites of polarized surface growth in budding yeast. *Current Biology*, *21*(23), 1994-1999.

Takatori, S., & Fujimoto, T. (2016). A novel imaging method revealed phosphatidylinositol 3,5-bisphosphate-rich domains in the endosome/lysosome membrane. *Commun Integr Biol*, *9*(2), e1145319. https://doi.org/10.1080/19420889.2016.1145319

Takeshige, K., Baba, M., Tsuboi, S., Noda, T., & Ohsumi, Y. (1992). Autophagy in yeast demonstrated with proteinase-deficient mutants and conditions for its induction. *The Journal of cell biology*, *119*(2), 301-311.

Tang, F., Kauffman, E. J., Novak, J. L., Nau, J. J., Catlett, N. L., & Weisman, L. S. (2003). Regulated degradation of a class V myosin receptor directs movement of the yeast vacuole. *Nature*, *422*(6927), 87-92. https://doi.org/10.1038/nature01453

Tang, F., Peng, Y., Nau, J. J., Kauffman, E. J., & Weisman, L. S. (2006). Vac8p, an armadillo repeat protein, coordinates vacuole inheritance with multiple vacuolar processes. *Traffic*, *7*(10), 1368-1377. https://doi.org/10.1111/j.1600-0854.2006.00458.x

Vicinanza, M., D'Angelo, G., Di Campli, A., & De Matteis, M. A. (2008). Function and dysfunction of the PI system in membrane trafficking. *Embo j*, *27*(19), 2457-2470. https://doi.org/10.1038/emboj.2008.169

Wallroth, A., & Haucke, V. (2018). Phosphoinositide conversion in endocytosis and the endolysosomal system. *Journal of Biological Chemistry*, *293*(5), 1526-1535. https://doi.org/10.1074/jbc.R117.000629

Weisman, L. S. (2003). Yeast vacuole inheritance and dynamics. *Annu Rev Genet*, *37*, 435-460. https://doi.org/10.1146/annurev.genet.37.050203.103207

Weisman, L. S., Bacallao, R., & Wickner, W. (1987). Multiple methods of visualizing the yeast vacuole permit evaluation of its morphology and inheritance during the cell cycle. *Journal of Cell Biology*, *105*(4), 1539-1547. https://doi.org/10.1083/jcb.105.4.1539

Wilson, Z. N., Scott, A. L., Dowell, R. D., & Odorizzi, G. (2018). PI(3,5)P2 controls vacuole potassium transport to support cellular osmoregulation. *Molecular Biology of the Cell*, *29*(14), 1718-1731. https://doi.org/10.1091/mbc.E18-01-0015

Winey, M., & O'Toole, E. T. (2001). The spindle cycle in budding yeast. *Nature Cell Biology*, *3*(1), E23-E27. https://doi.org/10.1038/35050663

Wishart, M. J., Taylor, G. S., & Dixon, J. E. (2001). Phoxy lipids: revealing PX domains as phosphoinositide binding modules. *Cell*, *105*(7), 817-820. https://doi.org/10.1016/s0092-8674(01)00414-7

Wurmser, A. E., & Emr, S. D. (2002). Novel PtdIns(3)P-binding protein Etf1 functions as an effector of the Vps34 PtdIns 3-kinase in autophagy. *J Cell Biol*, *158*(4), 761-772. https://doi.org/10.1083/jcb.200112050

Yau, R. G., Peng, Y., Valiathan, R. R., Birkeland, S. R., Wilson, T. E., & Weisman, L. S. (2014). Release from myosin V via regulated recruitment of an E3 ubiquitin ligase controls organelle localization. *Dev Cell*, *28*(5), 520-533. https://doi.org/10.1016/j.devcel.2014.02.001

# Appendix

**Table 2: The recipes of media, buffers, and reagents used in this thesis.**

| Name | Description |
|---|---|
| LiSORB | 100mM Lithium Acetate (LiOAc), 10mM Tris pH: 8.0, 1mM EDTA pH: 8.0, 1M Sorbitol (Merck, #107758), ddH2O to complete the desired volume. Filter to sterilize |
| LiPEG | 100mM LiOAc (Sigma, #L6883), 10mM Tris pH: 8.0, 1mM EDTA pH 8.0, 40% PEG3350 (Sigma, #P4338) ddH2O to complete the desired volume. Filter to sterilize. |
| P1 | 50mM Tris-HCl pH:8.0, 10mM EDTA pH 8.0, 0.1 mg/mL RNase A |
| P2 | 200mM NaOH, 1% SDS |
| P3 | 3M KAc pH: 5.5 |
| 1X PBS | 137mM NaCl, 2.7mM KCl (Merck, #104936), 10mM $Na_2HPO_4$ (Merck, #106575), 1.76mM $KH_2PO_4$ (Fisher BioReagents, #BP362). Adjust pH to 7.2-7.4 |
| 1X TAE buffer | 4.84 g of Tris, 1.14 mL of Glacial acetic acid (Isolab, #901016), 2 mL of 0.5M EDTA pH:8.0 (Sigma, #E5134), ddH2O up to 1000 mL. |
| 2mM dNTP | 20 µL of dATP (100 mM), 20 µL dCTP (100 mM), 20 µL dTTP (100 mM) and 20 µL dGTP (100 mM), 920 µL ddH2O |
| SC-X; X= *URA, LEU, HIS or TRP* | 3.4 g of Bacto Yeast Nitrogen Base (YNB) without amino acids with ammonium sulfate, 1 g of SC-X dropout amino acid mix, 10 g of D- (+)-Glucose, 0.05 g of Adenine hemisulfate salt (Sigma # A9126), ddH2O up to 500 mL |
| YPAD | 5 g of Yeast Extract, 10 g of Peptone (Conda, #1616), 10 g of D-(+)-Glucose, 0.05 g of Adenine hemisulfate salt, ddH2O up to 500 mL |
| YPD with selective antibiotics (Geneticin, Nourseothricin, or Hygromycin) | 10 g of Yeast Extract, 20 g of Peptone, 20 g of D-(+)-Glucose, 20 g of Agar, ddH2O up to 1000 mL. 200 mg/L G418, 100 mg/L Nourseothricin or 300 mg/L Hygromycin in autoclaved agar. |

| | |
|---|---|
| TY agar | 5 g of NaCl, 5 g of Yeast Extract, 10 g of Tryptone, 20 g of Agar, ddH2O up to 1000 mL |
| TY liquid medium | 5 g of NaCl, 5 g of Yeast Extract, 10 g of Tryptone, ddH2O up to 1000 mL |
| $TY_{(l)}$ + antibiotics | 5 g of NaCl, 5 g of Yeast Extract, 10 g of Tryptone, ddH2O up to 1000 mL. 100 µg/mL Ampicillin or 50 Kanamycin µg/mL |
| TY agar + antibiotics | 5 g of NaCl (Merck, #106498), 5 g of Yeast Extract (Conda, #1702), 10 g of Tryptone (Biolife, #4122902), 20 g of Agar (Carl Roth, #5210.2), ddH2O up to 1000 mL. 100 µg/mL Ampicillin or 50 Kanamycin µg/mL |
| 10X PCR Buffer 1 | 500mM Tris-HCl (pH9.2), 160 mM $(NH_4)SO_4$, 17.5 mM $MgCl_2$ |
| 10X PCR Buffer 2 | 500mM Tris-HCl (pH9.2), 160 mM $(NH_4)SO_4$, 22.5 mM $MgCl_2$ |

**Table 3: The strain names and descriptions used in this thesis**

| **Name** | **Genotype** |
|---|---|
| **ESM356-1** | (Spore 2.1) *MATa ura3-52 leu2Δ1 his3Δ200 trp1Δ63* |
| **MUK074-1** | ESM356-1 *VPH1-3xmCherry-kanMX6 ATG18-mNeongreen-hphNT1* |
| **MUK080-1** | ESM356-1 *VPH1-3xmCherry-kanMX6 ATG18-mNeongreen-hphNT1 vac14Δ::klTPR1* |
| **MUK081-1** | ESM356-1 *VPH1-3xmCherry-kanMX6 ATG18-mNeongreen-hphNT1 vac7Δ::klTPR1* |
| **MUK087-1** | ESM356-1 *VPH1-3xmCherry-kanMX6 SCH9-mNeongreen-hphNT1* |
| **MUK088-1** | ESM356-1 *VPH1-3xmCherry-kanMX6 IVY1-mNeongreen-hphNT1* |
| **MUK089-1** | ESM356 *VPH1-3xmCherry-kanMX6 atg18Δ::ATG18-mNeongreen-hphNT1* |
| **MUK090-1** | ESM356 *VPH1-3xmCherry-kanMX6 atg18Δ::atg18-FGGG -mNeongreen-hphNT1* (60-4) |
| **MUK091-2** | ESM356 *VPH1-3xmCherry-kanMX6 atg18Δ::atg18-SLOOP-mNeongreen-hphNT1* (61-3) |
| **MUK110-1** | MUK080-1 (SEY063(ESM356-1 - VPH1-mcherry-kan) ; ATG18-mNeongreen-hygromycin + vac14::TRP) *leu2::LEU2-fab1-ha***fab1-ha-leu pSE003** |
| **MUK098** | MUK089-1 *leu2::LEU2-fab1-ha* (CDY59 (CDY53-1(Atg18Δ hyg vph1-mcherry kan) Atg18-GFP (klTRP3)) + ATG18-mNeongreen-hygromycin. GFP is exchanged with mNeongreen. (59-2)) ***fab1-ha-leu pSE003*** |
| **MUK111-1** | MUK090-1 *leu2::LEU2-fab1-ha*(CDY60 (CDY53-1(Atg18Δ hyg vph1-mcherry kan) Atg18-FGGG-GFP (klTRP3)) + ATG18-mNeongreen- |

| | |
|---|---|
| | hygromycin. GFP is exchanged with mNeongreen. ) **fab1-ha-leu pSE003** |
| **MUK110-1** | MUK080-1 (SEY063(ESM356-1 - VPH1-mcherry-kan) ; ATG18-mNeongreen-hygromycin + vac14::TRP) *leu2::LEU2-fab1-ha***fab1-ha-leu pSE003** |
| **MUK113** | MUK081-1 *leu2::LEU2-fab1-ha*(SEY063(ESM356-1 - VPH1-mcherry-kan) ; ATG18-mNeongreen-hygromycin + vac7::TRP) **fab1-ha-leu pSE003** |
| **MUK111-1** | MUK090-1 *leu2::LEU2-fab1-ha*(CDY60 (CDY53-1(Atg18Δ hyg vph1-mcherry kan) Atg18-FGGG-GFP (klTRP3)) + ATG18-mNeongreen-hygromycin. GFP is exchanged with mNeongreen. ) **fab1-ha-leu pSE003** |
| **SGY008-1** | ESM356 *VPH1-3xmCherry-kanMX6 FAB1-inserted into mNeongreen-hygromycin hphNT1 (pMUK003-1). Later this cassette transformed into SEY063(ESM356-1 ((Spore 2.1) MATa ura3-52 leu2Δ1 his3Δ200 trp1Δ63 - VPH1-mcherry-kan. Confirmed by microscopy). Verified by fluorescence microscopy analysis. (2nd colony from the patch)* |
| **MUK113** | MUK081-1 *leu2::LEU2-fab1-ha*(SEY063(ESM356-1 - VPH1-mcherry-kan) ; ATG18-mNeongreen-hygromycin + vac7::TRP) **fab1-ha-leu pSE003** |
| **SGY009-1** | ESM356 *VPH1-3xmCherry-kanMX6 VAC14-mNeongreen-hphNT1*VAC14 inserted into mNeongreen-hygromycin (pMUK003-1). Later this cassette transformed into SEY063(ESM356-1 ((Spore 2.1) MATa ura3-52 leu2Δ1 his3Δ200 trp1Δ63 - VPH1-mcherry-kan. Confirmed by microscopy). Verified by fluorescence microscopy analysis. |

| | |
|---|---|
| **SGY008-1** | ESM356 *VPH1-3xmCherry-kanMX6 FAB1-inserted into mNeongreen-hygromycin hphNT1 (pMUK003-1). Later this cassette transformed into SEY063(ESM356-1 ((Spore 2.1) MATa ura3-52 leu2Δ1 his3Δ200 trp1Δ63 - VPH1-mcherry-kan. Confirmed by microscopy). Verified by fluorescence microscopy analysis. (2nd colony from the patch)* |
| **MUK117-1** | AKY4003-1(ESM356 *VAC7-GFP-HIS3MX6. Vacuole signal confirmed by microscopy.) VPH1-3mCherry-natNT1t.* Confirmed by microscopy |
| **SGY009-1** | ESM356 *VPH1-3xmCherry-kanMX6 VAC14-mNeongreen-hphNT1*VAC14 inserted into mNeongreen-hygromycin (pMUK003-1). Later this cassette transformed into SEY063(ESM356-1 ((Spore 2.1) MATa ura3-52 leu2Δ1 his3Δ200 trp1Δ63 - VPH1-mcherry-kan. Confirmed by microscopy). Verified by fluorescence microscopy analysis. |

**Table 4: The primers and their sequences used in this thesis**

| **Primer Name** | **Sequence (5' to 3')** |
|---|---|
| **NeongreenS3 linker-fw** | AGGTCGACGGATCGGTGCCGGTGCTGGTTCCATTTCAATGGTGA GTAAAGGCGA |
| **NeongreenS3 -linker-rev** | TCGCCTTTACTCACCATTGAAATGGAACCAGCACCGGCACCGAT CCGTCGACCT |
| **SeqForNeon green** | GTCGTTAGAACGCGGCTAC |
| **NeongreenP ntMUT2-FW** | GTCGACGGATCGGCCGGTGCTGGT |
| **NeongreenP ntMUT2-Rev** | ACCAGCACCGGCCGATCCGTCGAC |
| **VAC7-S3** | AAAAATCTACGGCTATTCAAAAGGATTCCATGGTCCATCCTGGT AAGAAGCGTACGCTGCAGGTCGAC |
| **VAC7-S2** | AAAAAGAAAAATACCCAGCTTTGACGAAAAAGCTACATTCTTA ACACTCAATCGATGAATTCGAGCTCG |
| **VAC7-S1** | TTATCGTTTCATCTCAGGCAAGTTAAAGCATTTGGGAAACGTGC TAGATGCGTACGCTGCAGGTCGAC |
| **VAC7-2** | ACTATCGCTTCCGCTACTA |
| **VAC7-1** | TGTAAGTCTTCCTGGCCAC |
| **VAC7-int-rev;** | GCACCAGTGCTAATATGTCT |
| **VAC14-S3** | ATAGTGGCAGTCTGCCATTCAACCGCAATGTATCCGATAAATTA AAAAAACGTACGCTGCAGGTCGAC |
| **VAC14-S2** | CAGGTCCATTTCTTAACCAAAGATGCTTTCAATCAGGTAATGGG TAGTTAATCGATGAATTCGAGCTCG |
| **VAC14-S1** | TTGATGCTGCTGTGCTTATCTGCTCAGGCTACAACAGGAACTGG AACATGCGTACGCTGCAGGTCGAC |
| **VAC14-2** | TACGCAGATCCGTCGCGA |
| **VAC14-1** | GTCCTATCAGCAGCTAACG |

| | |
|---|---|
| **Vac14-int-rev;** | TCATCAGTCTCCATACTCAG |
| **FAB1-S1** | AATAGCAAGGTAGCTTCCATCCTGTACATGCAAGACCGTCACAC AGCATGCGTACGCTGCAGGTCGAC |
| **FAB1-S2** | AGTGTATAAAAAAAAGTTACAGAATATAACTTGTACACGTTTAT GTATTAATCGATGAATTCGAGCTCG |
| **FAB1-S3** | TGGAGAGGTATATTTTGATGGTTCCTGATCCGTGGTATAGGGAA GGAAATCGTACGCTGCAGGTCGAC |
| **Fab1-fw2** | TGTTGACTCTCTCTAACTCT |
| **fab1-2-sac2** | TCTCCGCGGCGCAGGTTCGAATCCTGT |
| **Fab1-int-rev** | CGTATGTGTCTGCATGCTCA |
| **IVY1-S2** | TCACTTTCTCCATTTCTATATAAAAAGCATACATAGAGTTACAA ATTTTAATCGATGAATTCGAGCTCG |
| **IVY1-S3** | ACAATCACAGCAGCGATACGGACGGCATGCAAGACCAGTCAAG TAATATACGTACGCTGCAGGTCGAC |
| **IVY1-1** | ATGGTCAATGCGGGCAAAAG |
| **IVY1-2** | GTGCTGACAAATTACTCGCG |
| **SCH9-S3** | ACGGCGACCAACACATGGATGACGAATTTGTCAGTGGAAGATT CGAAATACGTACGCTGCAGGTCGAC |
| **SCH9-S2** | AAAAGAAAAGGAAAAGAAGAGGAAGGGCAAGAGGAGCGATTG AGAAATCAATCGATGAATTCGAGCTCG |
| **Sch9-1** | GTTGTGCTCAGCTCATCC |
| **Sch9-2** | AGCAGTGATTATGAGACGTG |
| **ATG18-S2** | GTGTATGCGTTGTGACGTACGGAAGGCAGCGCGAGACACTTCC GTGATCAATCGATGAATTCGAGCTCG |
| **ATG18-s3** | AGAGAGGCGGCGATTGCTTAATATTGTCACAGTATTCCATCTTG ATGGATCGTACGCTGCAGGTCGAC |

**Table 5: The plasmids and their descriptions used in this thesis**

| Name | Description |
|---|---|
| pFA6a-mNeonGreen-KanMX | From addgene # 129099. |
| pMUK001 | pFA6a-mNeonGreen-KanMX site directed mutagenized (site directed mutagenesis protocol applied with primers `NeongreenS3linker-fw`(7-75) and `NeongreenS3-linker-rev`(7-76). Confirmed by Sanger Sequencing with primer `SeqForNeongreen`(7-77). Amplified with miniprep protocol. |
| pMUK002 | pFA6a-mNeonGreen-KanMX site directed mutagenized once again(May be used with S2/S3 primers to fuse mNeonGreen with selective marker kanamycin) mNeongreen linker sequence is mutagenized with site directed mutagenesis pMUK001-1 plasmid with primers `NeonGreenPntMUT2-FW` and `NeonnGreenPntMUT2-Rev`. Confirmed in vivo by fusing mNeongreen with BFA1 gene. We saw `green` signal with GFP setup where BFA1 localizes on SPB. |
| pFA6a-HISmX6 | pFA6a-His3MX6. The length of casette PCR product for S1 and S2 primers is 1347bp. |
| pKS134 | pFA6a-natNT2. NatMX4 disruption cassette. 334 bp PCR fr. of pEG202 cloned via XhoI/SacI into pKS129 (natMX4-Stop-XhoI). Control digestion with NotI: exp. fr. 2390+1394 bp. |
| pKS133 | pFA6a-hphNT1 |
| pMUK003 | pFA6a-mNeonGreen-hphNT1 (May be used with S2/S3 primers to fuse mNeonGreen with selective marker hygromycin) Selection marker of pKS133\(EcoRV-BglII), size 1700bp, subcloned to pMUK002-1(EcoRV-BglII), backbone size 3400 bp. Confirmed by double digestion w/EcoRVand BglII: the sizes were 3400 and 1700bp. Later |

| | |
|---|---|
| | confirmed by microscopy; fusion with BFA1 showed SPB localization. |
| pSE003 | prs305-fab1 hyperactive. From pse002, using xho1 and sac2 restriction sites; subcloned to prs305 backbone. Eco 911 is used to linearized and integrate to leu locus.Confirmation is done via xho1 and sac1 enzymes. Backbone: 3.5 kb and insert is 7.25 kb |

Permission for figure 1-4 is granted with the license number of 5637091335738 on 27/09/2023. The permission is available with the following link: https://s100.copyright.com/CustomerAdmin/PLF.jsp?ref=f4e9fd27-b11a-4545-826c-4be7315362c0

Permission for figure 1-6 is granted with the license number of 5636051183082 on 25/09/2023. The permission is available with the following link: https://s100.copyright.com/CustomerAdmin/PLF.jsp?ref=e14829ca-fc1c-439c-839d-8174431fea2c